Design Optimization of LNAs and Reflectarray Antennas Using the Full-Wave Simulation-Based Artificial Intelligence Models with the Novel Metaheuristic Algorithms

Filiz Güneş, Salih Demirel, and Selahattin Nesil

Abstract In this chapter, the two primarily important highly nonlinear design problems of the contemporary microwave engineering which are "Low Noise Amplifier (LNA)"s and "Reflect-array Antenna (RA)"s are solved as "Design Optimization problems." For this purpose, firstly the design problem is defined in terms of the feasible design variables (FDVs), the feasible design target space (FDTS), both of which are built up by integrating the artificial intelligence black-box models based upon the measurements or full-wave simulations and a suitable metaheuristic search algorithm. In the second stage, feasible design target (FDT) or objective function of the optimization procedure is determined as a sub-space of the FDTS. Thirdly, the cost function evaluating the objective is minimized employing a suitable metaheuristic search algorithm with respect to the FDVs. Finally the completed designs are verified by the professional Microwave Circuitor3-D EM simulators.

Keywords Microwave engineering • Low-noise amplifier • Reflectarray • Full-wave simulation • Artificial intelligence • Metaheuristic search algorithm • Feasible design target space • Feasible design variables

MSC codes: 78-01, 68-04, 94-01

F. Güneş (✉) • S. Demirel • S. Nesil
Department of Electronics and Communication Engineering, Yildiz Technical University, Esenler, Istanbul 34220, Turkey
e-mail: gunes@yildiz.edu.tr; fgunes51@gmail.com

S. Koziel et al. (eds.), *Simulation-Driven Modeling and Optimization*,
Springer Proceedings in Mathematics & Statistics 153,
DOI 10.1007/978-3-319-27517-8_11

1 Design Optimization of LNAs

1.1 LNA Design Problem

As the electronic industry moves towards higher integration and lower cost, RF and wireless design demands increasingly more "concurrent" engineering. Typically, today's most receivers are hand-held or battery-operated devices; one of the major challenges in these receivers is to design a low-noise amplifier (LNA) that has very low power consumption and operates from a very low supply voltage with the provided trade-off of noise measure and mismatch losses. Since the two transistor configurations consume more power from the higher voltage supply than the single transistor configurations, the two transistor configurations are unsuitable for this type of applications. Thus, after selection of a transistor among the available high technology transistors, then a low-noise design approach consists of trading off among the often contrasting goals of low noise, high gain, and input and output match within the device operation domain.

The design optimization method used for a microstrip LNA is given in a flow chart in Fig. 1. However the method can easily be applied to the LNAs using different wave guiding systems.

1.2 Feasible Design Target Space (FDTS)

Since the design optimization of an LNA necessitates the physical limits and compromise relations of the design hexagon consisting of bias voltage V_{DS}, bias current I_{DS}, noise F, gain G_T, input VSWR V_{in}, and output VSWR V_{out} belonging to the employed transistor, in the other words, the "Feasible Design Target Space (FDTS)" must be constructed as an important stage of the design optimization procedure. Certainly, within the optimization process, one can easily embed the desired performance goals without knowing the physical realizability conditions and compromise relations appropriately, but in this case, the device is utilized either under its performance potential or unrealizable requirements that result in failure in the design.

The block diagram of the FDTS is given in Fig. 2 where all the compatible performance quadrates (noise figure F, input VSWR V_{in}, output VSWR V_{out}, transducer gain G_T); the corresponding operation bandwidth B and the source Z_S and load Z_L terminations are obtained as the continuous functions of the device's operation parameters which are bias condition (V, I) and frequency at a chosen configuration type. Let us consider the most commonly used configuration which is common source configuration. Firstly a soft model of the transistor is constructed using either a suitable artificial intelligent network or an equivalent circuit built by a parameter extraction method to obtain the device's scattering S and noise N parameters as the continuous functions of the operation parameters V_{DS}, I_{DS}, f. Typical works for the S and N parameters modeling of a microwave transistor can

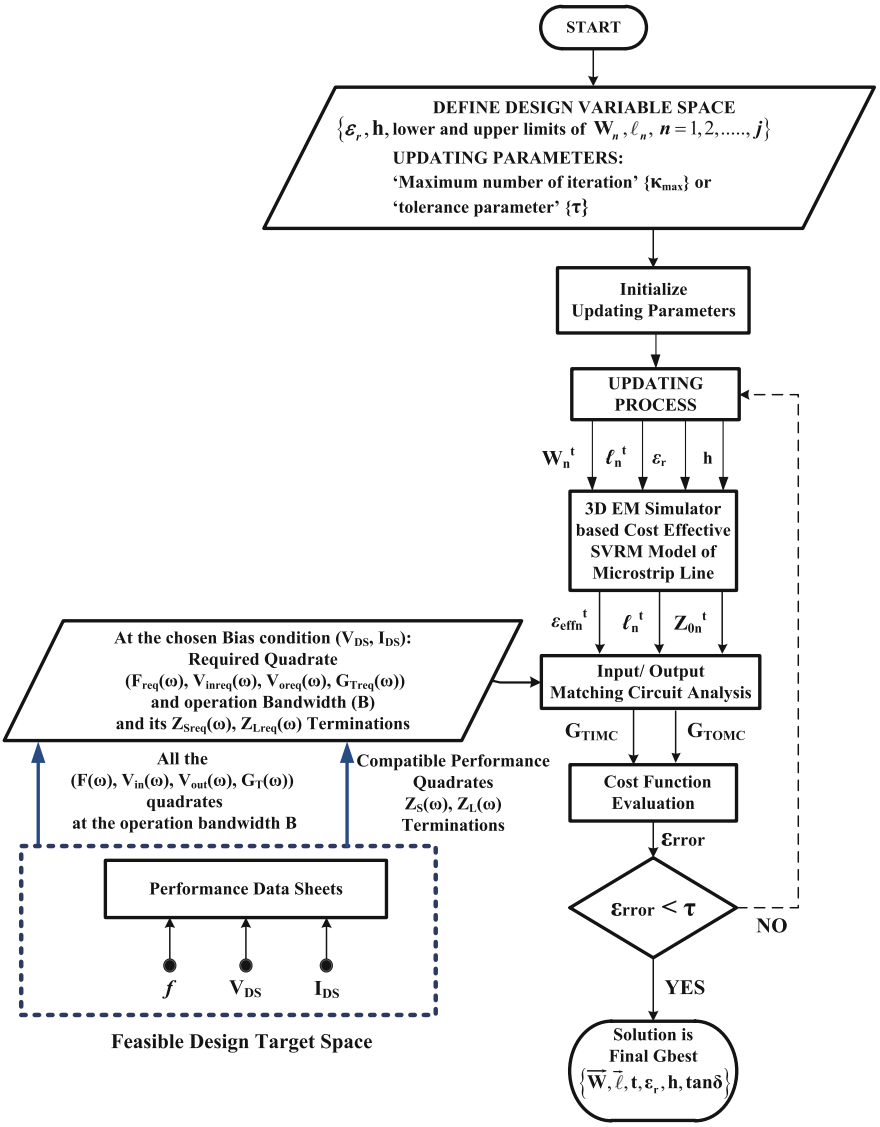

Fig. 1 Design flow chart of the microstrip LNA

be found in [1–7]. Secondly, potential performance of the microwave transistor is analyzed in terms of the S and N parameters at a chosen bias condition. This analysis has been achieved by solving the highly nonlinear performance equations of the transistor using either the analytical approaches based on the constant performance ingredient circles [8–14] or optimization methods without using the complicated microwave theory [15–17].

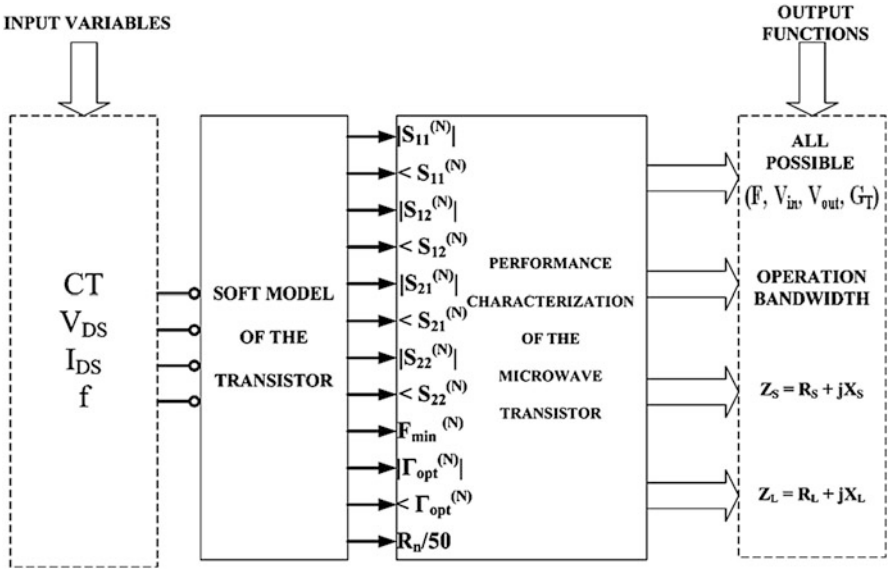

Fig. 2 Block diagramme for performance data sheets

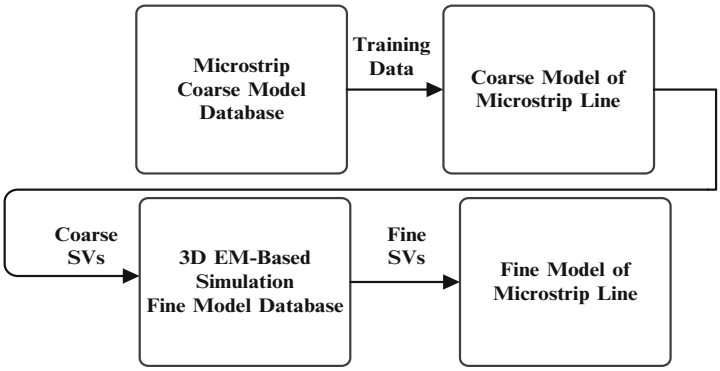

Fig. 3 3D EM simulation-based SVRM model of the microstripline

1.3 Feasible Design Variables (FDVs)

The second stage is modeling of the feasible design variables (FDVs) using the 3-D EM simulation-based support regression vector machine (SVRM). In this modeling, one-to-one mapping is built between the input domain consisting of the microstrip width W, substrate (ε_r, h) parameters, and frequency *f*, and the output domain defined by the equivalent transmission line parameters which are the characteristic impedance Z_0 and effective dielectric constant ε_{eff} (Fig. 3) [18, 19].

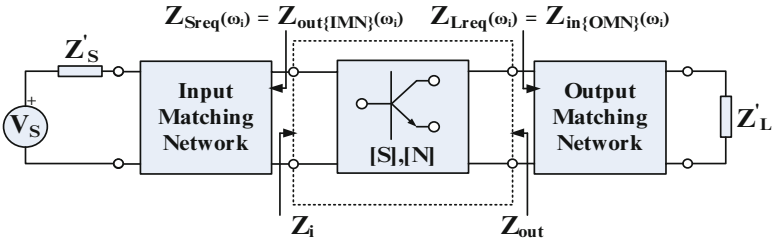

Fig. 4 Transistor with the input and output matching circuits of the compatible performance terminations Z_S, Z_L, respectively

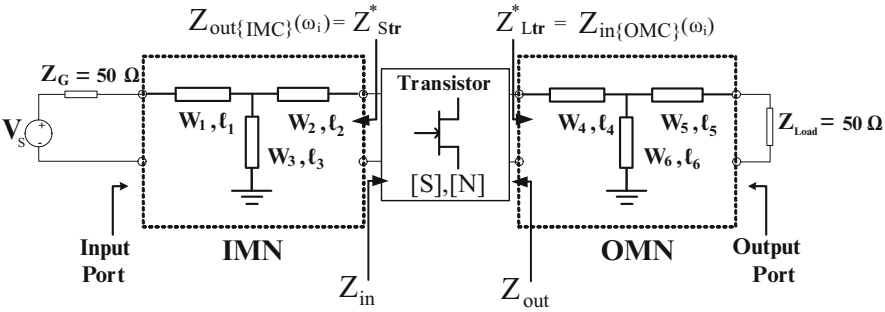

Fig. 5 LNA with the T-type microstrip matching networks

1.4 Design of Input and Output Matching Circuits

Final stage is the design of the input and output matching circuits. Transistor with the Darlington equivalencies of the compatible performance terminations Z_S, Z_L are given in Fig. 4. Input IMC and Output Matching Circuit (OMCs) are designed using either the gain or port impedance optimization of the two independent matching circuits given in Fig. 5 by either a gradient or metaheuristic algorithm. In the next subsection design strategies of LNA are given briefly.

1.5 Design Strategies

Here to fore the two different design strategies can be put forward for the LNAs: In the first strategy, considering $F(Z_S)$ and $V_{in}(Z_S, Z_L)$ as the free variables, $G_{Tmin} \leq G_T \leq G_{Tmax}$ and the corresponding termination Z_S, Z_L couple are determined solving the nonlinear transistor's performance equations with either analytical approaches using the constant performance ingredient circles or a constrained optimization problem. Thus, with the resulted V_{out}, the FDTS can be built consisting of the compatible ($F \geq F_{req}$, $V_{in} \geq 1$, $V_{out} \geq 1$, $G_{Tmin} \leq G_T \leq G_{Tmax}$) and the associated Z_S, Z_L terminations [8–11, 15, 16].

In the second strategy, only noise $F(Z_S)$ is considered as a free variable and the nonlinear performance equations are solved for the input termination Z_S satisfying simultaneously both the maximum gain G_{Tmax} and the required noise F, again either in the analytical way or as a constrained maximization problem. Then the load Z_L is obtained by the conjugate-matched output port $V_{out} = 1$ condition. Mismatching at the input port can be adjusted by degrading either noise and mismatching at the output port. Thus a different FDTS can be built up consisting of the compatible ($F \geq F_{req}$, $V_{in} \geq 1$, $V_{out} \geq 1$, $G_{Tmin} \leq G_T \leq G_{Tmax}$) and the associated Z_S, Z_L terminations [12–14, 17].

Both design strategies are based on the following balance equation:

$$\left(1 - \left|\frac{V_{in}\,(Z_S, Z_L) - 1}{V_{in}\,(Z_S, Z_L) + 1}\right|^2\right) .G_{op}\,(Z_L) = \left(1 - \left|\frac{V_{out}\;(Z_S, Z_L) - 1}{V_{out}\,(Z_S, Z_L) + 1}\right|^2\right) .G_{av}\,(Z_S) \tag{1}$$

Where $G_{op}(Z_L)$ and $G_{av}(Z_S)$ are the operation and available power gains, respectively, which will be taken into account in the study case. Typical LNA designs based on these design strategies using either gradient or metaheuristic algorithms can be found in [20–26]. In the next section, a front-end amplifier design worked out by our research group in [26] will briefly be given as a case study based on the above methodology.

1.6 Case Study: HBMO Design Optimization of an LNA with Support Vector Microstrip Model

In this section, a HBMO design optimization procedure is given in subject to the design flow chart in Fig. 1 for a front-end amplifier so that all the matching microstrip widths, lengths $\{\{\vec{W}, \vec{\ell}\}\}$ can be obtained to provide the (Z_S, Z_L) terminations on a given substrate (ε_r, h, tanδ) for the maximum power delivery and the required noise over the required bandwidth of a selected transistor, respectively [26]. Thus, in the following subsection all the stages of the design procedure will be considered.

1.6.1 Feasible Design Target (FDT)

In this LNA design optimization problem, the design objective is to ensure the maximum output power delivery and the required noise. Thus, hereafter the problem of determination of the source impedance $Z_S = r_S + jx_S$ of a microwave transistor can be described as a mathematically constrained optimization problem so that the transducer gain $G_T(r_S, x_S, r_L, x_L)$ will be maximized simultaneously satisfying the required noise figure $F(r_S, x_S)$ provided that the stability conditions

are ensured at each sample frequency throughout the required operation bandwidth. The transistor's load impedance Z_L can be determined using the balanced Eq. (1) by the conjugate-matched output, that is, $V_{out} = 1 \iff Z_L = Z^*_{out}(Z_S)$. Thereby the multi-objective cost function of this constrained optimization process can be expressed as:

$$Cost\,(r_S, x_S,\, f_i) = e^{-\psi_1 G_{AV}(r_S,\, x_S, f_i)} + \psi_2 \left| F\,(r_S,\; x_S, f_i) - F_{req}\,(f_i) \right| \tag{2}$$

with the following constraints for the physical limits and stability of the transistor

$$\Re e\,\{Z_S\} > 0,\; \Re e\,\{Z_L\} > 0,\; F_{req} \geq F_{\min} \tag{3}$$

$$\Re e\,\{Z_{in}\} = \Re e\left\{ z_{11} - \frac{z_{12}\, z_{21}}{z_{22} + Z_L} \right\} > 0,\; \Re e\,\{Z_{out}\} = \Re e\left\{ z_{22} - \frac{z_{12} z_{21}}{z_{11} + Z_S} \right\} > 0 \tag{4}$$

Here the performance measure G_T, G_{AV}, and F functions can be expressed in terms of the transistor's z-parameters and Z_S, Z_L terminations as follows [27]:

$$G_T = \frac{P_L}{P_{avs}} = G_{AV}\,(Z_S)\;.M_{out}\,(Z_S,\; Z_L) \tag{5}$$

where

$$G_{AV}\,(Z_S) = \frac{|z_{21}|^2}{|z_{11} + Z_S|^2} \frac{r_S}{r_{out}},\; r_{out} \triangleq Re\,\{Z_{out}\},$$

$$M_{out}\,(Z_S, Z_L) = 1 - \left| \frac{Z_{out} - Z^*{}_L}{Z_{out} + Z_L} \right|^2 \leq 1, \tag{6}$$

$$F\,(Z_S) = \frac{\left(S/N\right)_i}{\left(S/N\right)_o} = F_{min} + \frac{R_n \left| Z_S - Z_{opt} \right|^2}{\left| Z_{opt} \right|^2 r_S} \tag{7}$$

Besides, ψ_1 *and* ψ_2 in the Eq. (2) are the weighting coefficients which can be chosen during the optimization process by trial, which in our case are taken as unity. Thus, the smaller cost is the fitter optimization process we have.

Here, for the ultra-wideband LNA design, the three alternatives are considered for the required noise figure F_{req} f of the selected transistor NE3512S02 using the honey bee mating optimization (HBMO): (1) $F_{req}(\omega_i) = F_{min}(\omega_i)$; (2) $F_{req}(\omega_i) = \text{constant} = 1.0$ dB; (3) $F_{req}(\omega_i) = \text{constant} = 1.5$ dB (Fig. 6).

In Fig. 6, the maximum gain variations of the transistor NE3512S02 for the matched output against the input mismatching V_{in} are given as compared with the analytical counterparts [14, 15]. Besides the corresponding terminations of the maximum gain for the matched output and $F(f) = 1$ dB are given in Tab. 1.

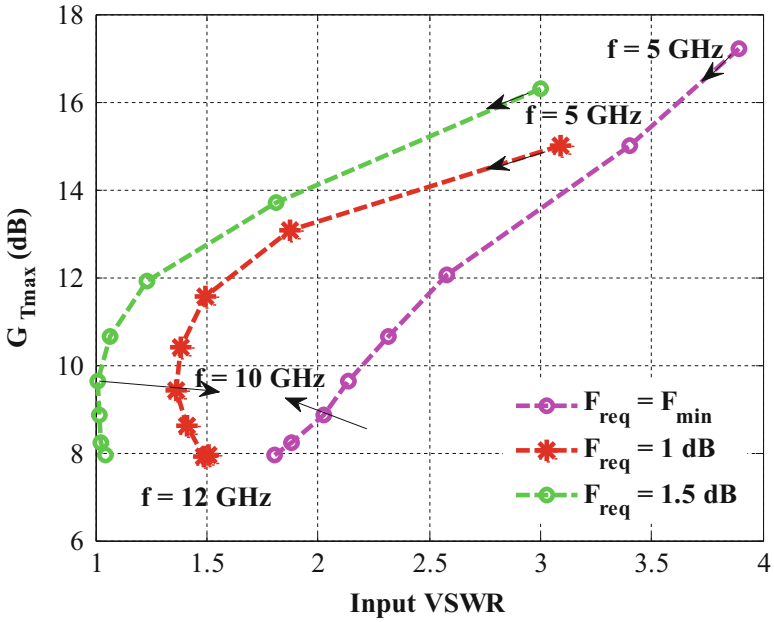

Fig. 6 Maximum gain against input VSWR Vin and for $|\rho_{out}| = 0$ for NE3512S02 at the bias condition $V_{DS} = 2$ V, $I_{DS} = 10$ mA

Table 1 The source Z_S and load Z_L terminations for the maximum gain for $|\rho_{out}| = 0$ and $F(f) = 1$ dB for NE3512S02 at the bias condition $V_{DS} = 2$ V, $I_{DS} = 10$ mA

f(GHz)	V_{in}	G_{TMAX}(dB)	Real(Z_L) Ω	Imag(Z_L) Ω	Real(Z_S) Ω	Imag(Z_S) Ω
5	3.09	15.0	16.32	29.97	14.66	23.23
6	1.87	13.06	19.31	26.14	14.31	12.36
7	1.49	11.55	21.78	22.19	14.78	3.09
8	1.38	10.40	23.52	17.42	15.97	−5.00
9	1.36	9.43	25.35	12.18	18.08	−12.03
10	1.40	8.62	27.06	6.791	20.77	−18.72
11	1.49	7.92	29.34	0.872	24.72	−24.68
12	1.50	7.94	35.67	−5.91	35.37	−28.85

1.6.2 Design Objective for the Matching Networks

Thus, we have the transistor terminations solving the nonlinear performance equations subject to the objective of Eq. (2–7). A novel metaheuristic the HBMO is used in the solution procedure of the equations of Eq. (2–7) that will briefly be given in the following section. In the design optimization procedure, the gain of the input/output matching two-port terminated by the complex conjugate of the $(Z_S(\omega_i)/Z_L(\omega_i))$ as given in Fig. 5 is maximized over the required bandwidth:

$$cost\left(\vec{W},\ \vec{\ell}\right) = Minimum \sum_i \left(1 - G_{Ti}\left(f_i, \vec{W},\ \vec{\ell}\right)\right) \tag{8}$$

where $\left\{\vec{W},\ \vec{\ell}\right\}$ is the design variable vector which consists of the microstrip widths and lengths of the problem matching circuit and G_{Ti} is the transducer power gain of the same matching circuit at the sample frequency f_i. In the worked example, T-type matching circuits are considered to be designed. The proposed method can be applied without any difficulty to another different type of matching circuit. In that case, the gain function G_{Ti} given in Eq. (8) should be evaluated for the considered matching circuit.

1.6.3 Design Variables: Microstrip Widths and Lengths $\{W,\ \ell\}$

In this design optimization procedure, the microstrip widths and lengths $\left\{\vec{W},\ \vec{\ell}\right\}$ on a selected substrate $\{\varepsilon_r, h, tan\delta\}$ are directly used by the HBMO optimization of the LNA (Fig. 1) and the cost function (Eq. 8) is evaluated by means of the SVRM microstrip model (Fig. 1). The 3-D SONNET-based SVRM model of the microstrip [18, 19] is employed that provides an accurate, fast, and cost effective generalization from the highly nonlinear discrete mapping from the input domain M (R4) of the microstrip width W, substrate $\{\varepsilon_r, h, tan\delta\}$, and frequency f to the output domain of the characteristic impedance Z_0 and effective dielectric constant ε_{eff}.

Here, the range of input and output domains is given as $\{0.1\text{ mm} \le W \le 4.6\text{ mm}, 2 \le \varepsilon_r \le 10, 0.1\text{ mm} \le h \le 2.2\text{ mm}, 2\text{ GHz} \le f \le 14\text{ GHz}\}$ and $\{3\,\Omega \le Z_0 \le 240\,\Omega\}$ and $\{1.5 \le \varepsilon_{eff} \le 9.7\}$, respectively.

1.6.4 Building Knowledge-Based Microstrip SVRM Model

Knowledge-based microstrip SVRM is given as block diagram in Fig. 3 where the quasi-TEM microstrip analysis formula is used as a coarse SVRM model database by means of which $n_{freq} \times n_\varepsilon \times n_h \times n_w = 5 \times 5 \times 4 \times 10 = 1000$ $\left(\vec{x}_i, \vec{y}_i\right)$ data pairs are obtained to train the coarse SVRM, where n_{freq}, n_ε, n_h, n_w are the number of the samples for the frequency, the dielectric constant, the substrate height and width, respectively. Tab. 2 gives the accuracy of the "Z_0" coarse model with the number of the SVs and the radius of selection tube ϵ. 402 and 367 fine SVs obtained from 3-D SONNET simulator are used to train the fine "Z_0" and "ε_{eff}" SVRMs, respectively, with the accuracy at least 99.4 % (Fig. 7b). Thus the substantial

Table 2 Accuracy of the fine SVRM model

Epsilon (ϵ)	Number of SVs	Accuracy (%)
0.05	583	99.4
0.07	402	98.6
0.1	279	97.9

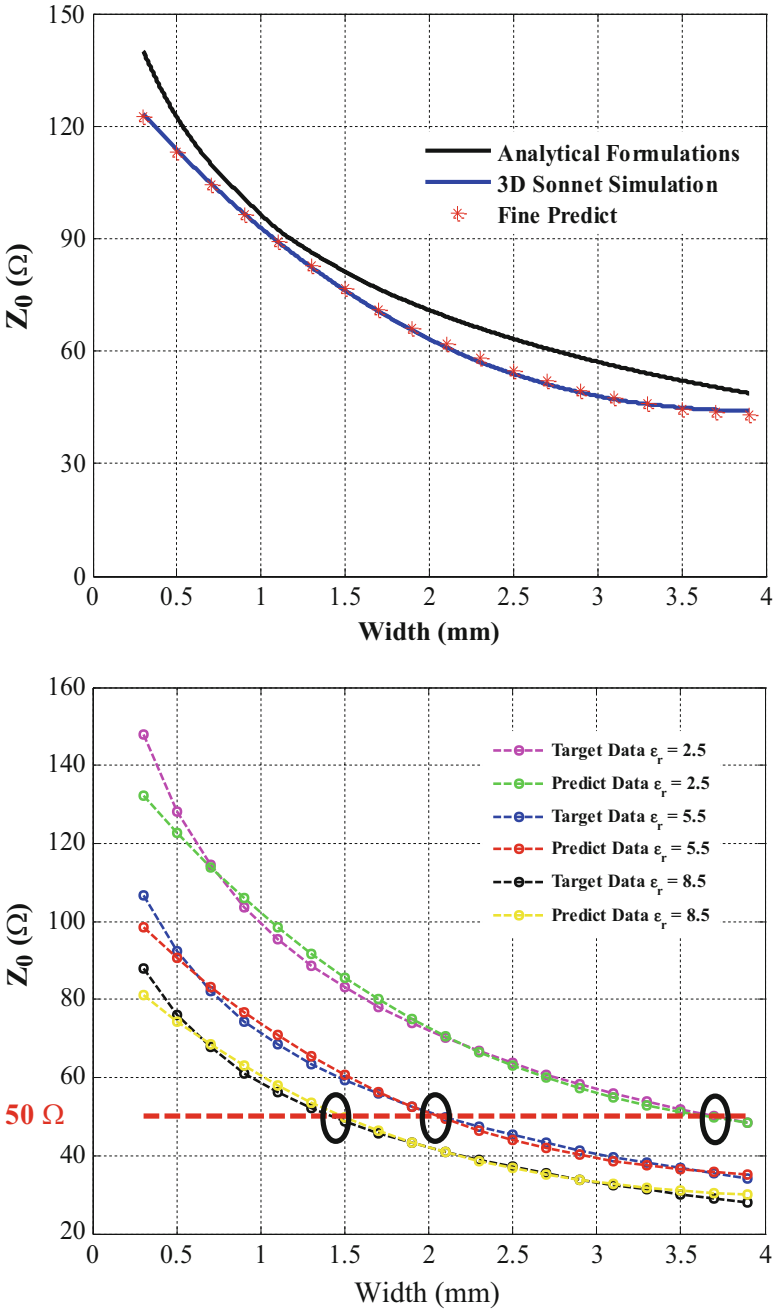

Fig. 7 (continued)

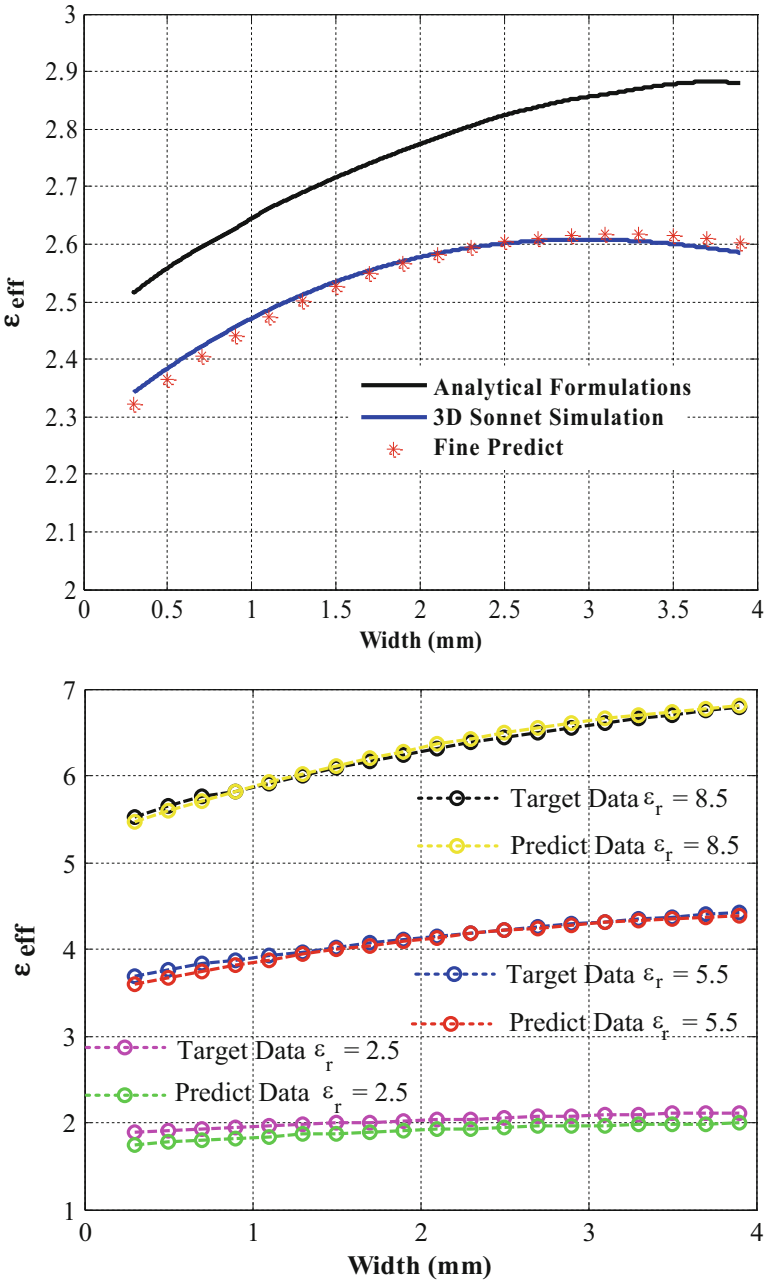

Fig. 7 Comparative variations for characteristic impedance Z_0 and effective dielectric constant ε_{eff} vs width of the analytical formulations, fine model and the 3-D SONNET simulation. (**a**) Rogers 435 ($\varepsilon_r = 3.48$, h = 1.524 mm, tanδ = 0.003, t = 0.001 mm) at 4 GHz, (**b**) Z_0 variations for various dielectrics at f = 8 GHz (**c**) Rogers 435($\varepsilon_r = 3.48$, h = 1.524 mm, tanδ = 0.003, t = 0.001 mm) at f = 4 GHz (**d**) ε_{eff} for various dielectrics at f = 8 GHz

reduction (up to 60 %) is obtained utilizing sparseness of the standard SVRM in number of the expensive fine discrete training data with the negligible loss in the predictive accuracy and the resulted fine microstrip SVRM model can be considered as accurate as the 3-D EM simulator and as fast as the analytical formulae. The typical comparative prediction curves of the microstrip SVRM model take place in Fig. 7a–d give Z_0 and ε_{eff} variations with respect to the microstrip width W resulted from the fine SVRM model for the dielectrics at f = 4GHz and 8 GHz, respectively.

1.6.5 HBMO with Royal Jelly for the Amplifier's Matching Network Design Problem

HBMO is a recent swarm-based optimization algorithm to solve highly nonlinear problems, whose based approach combines the powers of simulated annealing, genetic algorithms, and an effective local search heuristic to search for the best possible solution to the problem under investigation within a reasonable computing time.

The flow diagramme of the algorithm is given by Fig. 8. The user-defined parameters of the algorithms are the number of the Drone bees N_{Drone}, maximum iteration number t_{max}, sizes of the genetic inheritance of the Master Queen Q_M, and each Drone bee D_j, m_Q, m_D; maximum number of feeding times of the Master Queen Q_M with Royal Jelly N_{RJ}, maximum E_{max} and minimum E_{min} energies of the Queen at the start and end of the mating flights, respectively, and the required cost $cost_{req}$. In the algorithm, the numbers of the Hive N_{Hive}, Brood N_{Brood}, LarvaN_{Larva}, Fertilization $N_{fertilization}$ are set equal to N_{Gen} which is taken to be equal to t_{max} and the total egg number $N_{Egg} = (N_{Gen})$ 5.

The proposed HBMO algorithm is used effectively and efficiently to design a front-end amplifier. The working mechanism of the HBMO version can briefly be summarized as follows (Fig. 8): In the proposed HBMO algorithm, after initialization, a genetic pool is built by the mating process of a single queen with the drone bees, governed by the probabilistic annealing law, thus a complete solution space between the predefined lower and upper limitations is generated in the form of the queen's and the successful drones's genetic inheritances. Here the entire colony is divided into the N_{hive} hives that facilitates "Sorting" process applied to the sub-colonies step by step, in the other words the search for the new candidates is performed in reduced number of sub-matrices instead of making a search for a single gigantic matrix. This gains the algorithm both simplicity and efficiency. The mating process is also simplified to only energy-based probabilistic decision rule to enable the fittest solutions. Furthermore, a sub-solution space as the "Egg-Population" is built by crossover processing of the entire huge solution space of the genetic pool. Accelerated exploration in the form of the five steps is applied into the egg population to obtain the best solution: 1-Fertilization ($N_{fertilization}$), 2-Larva (N_{Larva}), 3-Brood (N_{brood}), 4-Hive (N_{Hive}), and 5-Generation (N_{Gen}), size of each of these steps is equal to maximum iteration number which is taken to be equal to 20 in our application. The accelerated exploration is based on the "sorting" step

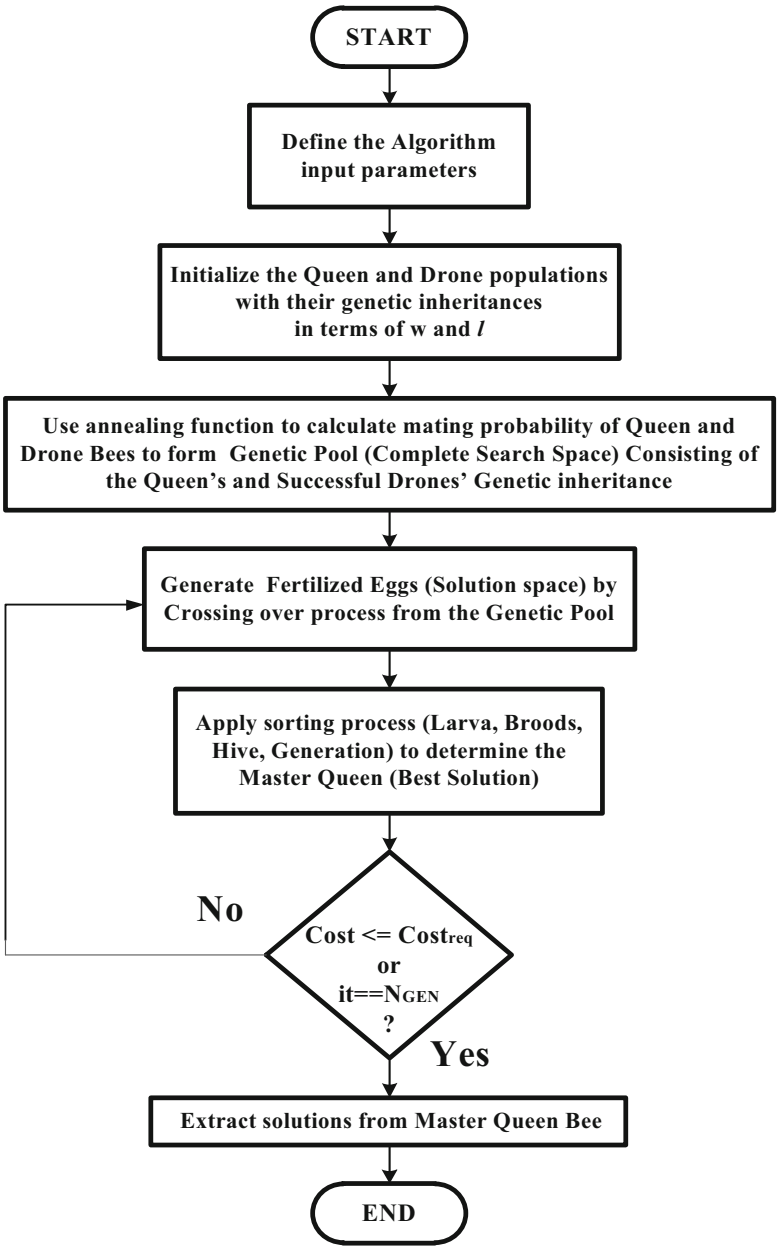

Fig. 8 Flow chart of the HBMO algorithm

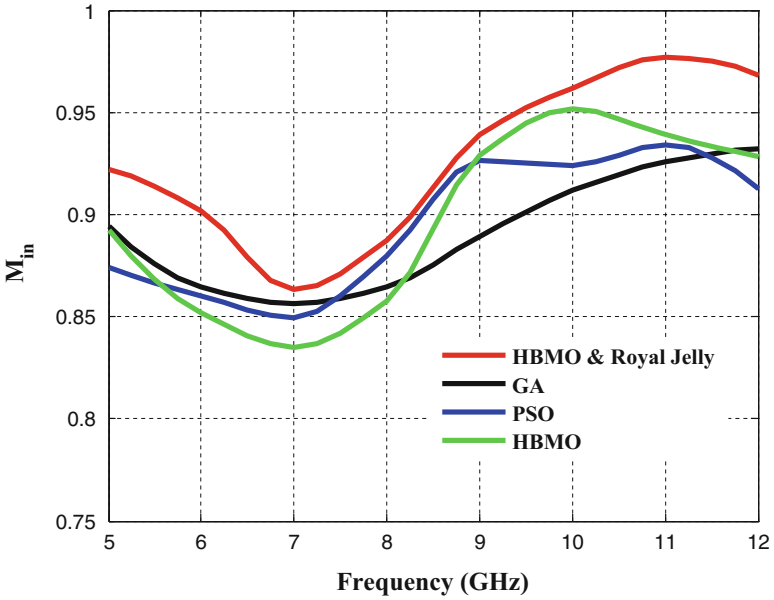

Fig. 9 Mismatching at the input port using standard metaheuristic algorithms

by step and can briefly be summarized as follows: In each step, the current entire population is divided into the subpopulations having (N_{Gen}) members, then the best member with the minimum cost value of each subpopulation is promoted to the next step, and the rest members are discarded. In this final step, only (W_j, ℓ_j) couples having the minimum cost of the competition will be chosen as the new Master Queen bee which will take new mating flights to give born to new members of the next generation of the colony. Besides "Royal Jelly" feed is used in algorithm to make a local search in order to improve the fitness of the Master Queen bee at the end of the each generation or iteration. Thus comparison with the counterpart population-based algorithms (Figs. 9, 10, 11, 13, 14 and 15) verified that a robust and fast convergent algorithm with the minimal problem information is resulted for the most successful design of a front-end amplifier.

1.6.6 Implementation

The user-defined parameters of the HBMO algorithms are set to the following values in the design of the front-end amplifier: $N_{Drone} = 20$, $t_{max} = N_{Gen} = 20$, $m_Q = 1000$, $m_D = 100$, $N_{Rj} = 1000$, $E_{max} = 1$, $E_{min} = 0.2$, $cost_{req} = 0.02$.

In the implementation, NE3512S02 is selected as the microwave transistor and maximum gain $G_{Tmax}(f)$ variations constrained by the minimum noise figures $F_{min}(f)$, F = 1 dB and F = 1.5 dB are evaluated numerically using the HMO and

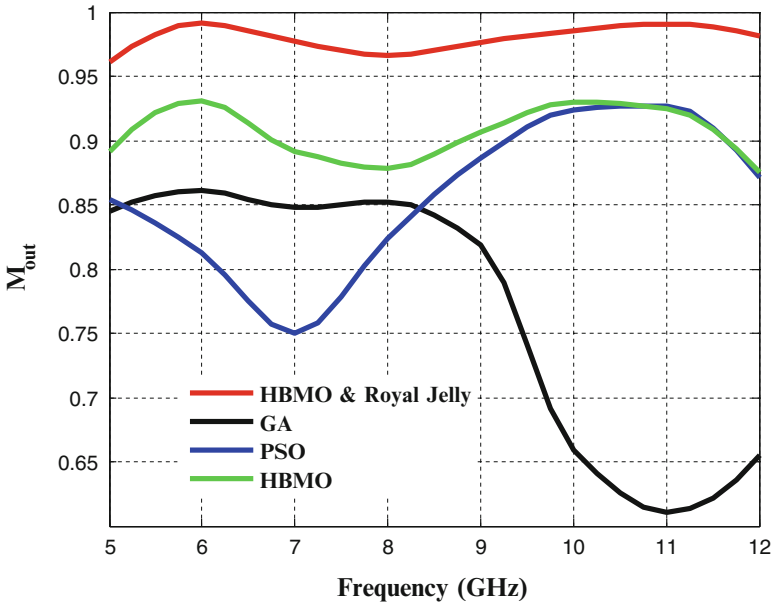

Fig. 10 Mismatching at the output port using standard metaheuristic algorithms

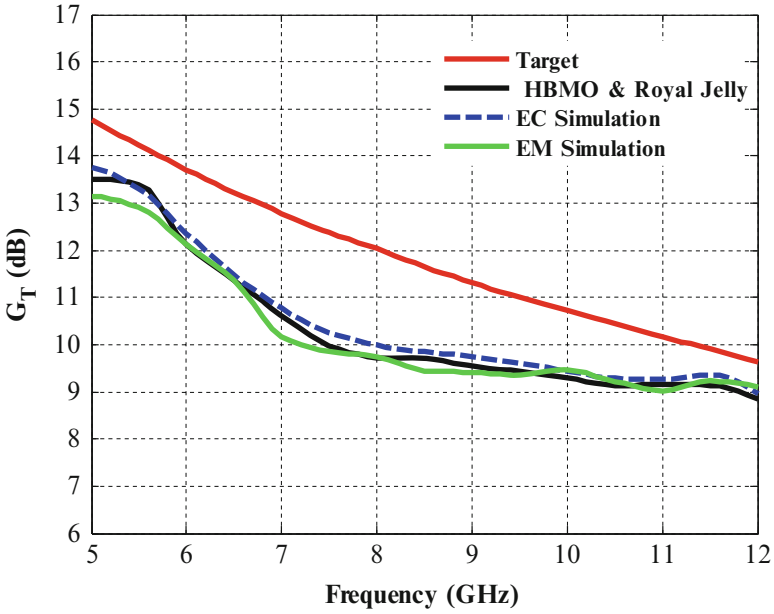

Fig. 11 Gain performance of the amplifier for the maximum power delivery for the noise figure F(f) = 1 dB

compared the analytical counterparts [14, 15] in Fig. 6 and the transistor source Z_S and load Z_L terminations are given for F = 1 dB in Tab. 1. The gain performance G_{Tmax} (f) constrained by F = 1 dB at the bias condition (2 V, 10 mA) is designed on the substrate of Rogers 4350 ($\varepsilon_r = 3.48$, h = 1.524 mm, tanδ = 0.003, t = 0.001 mm) along the bandwidth of 5–12 GHz. The solution space of the T-type matching circuits in Fig. 5 is shown in Tab. 2. Impedance mismatching at the input and output ports are given as compared with the genetic algorithm (GA), particle swarm optimization (PSO), and HBMO with and without Royal Jelly in Figs. 9 and 10, respectively. The resulted gain, noise performances, input and output reflections of the amplifier designed by HBMO with Royal Jelly take place by are given in Figs. 11, 12, 13, and 14, respectively, as compared with the targeted performances and obtained by the AWR circuit and 3-D EM simulators. Furthermore the cost and execution time with iteration number of the used counterpart's algorithms which are GA, PSO, and HBMO with and without Royal Jelly are given in Fig. 15. The optimization parameters of the studied algorithms are given in Tab. 5, the parameters of the PSO and GA are taken as their default values of the MATLAB optimization tool, MATLAB 2010b. The cost values and execution times at the 20th iteration of a random run are given in Tab. 3 performed by the Intel Core i7 CPU, 1.60 GHz Processor, 6 GB RAM (Tabs. 4, 5 and 6).

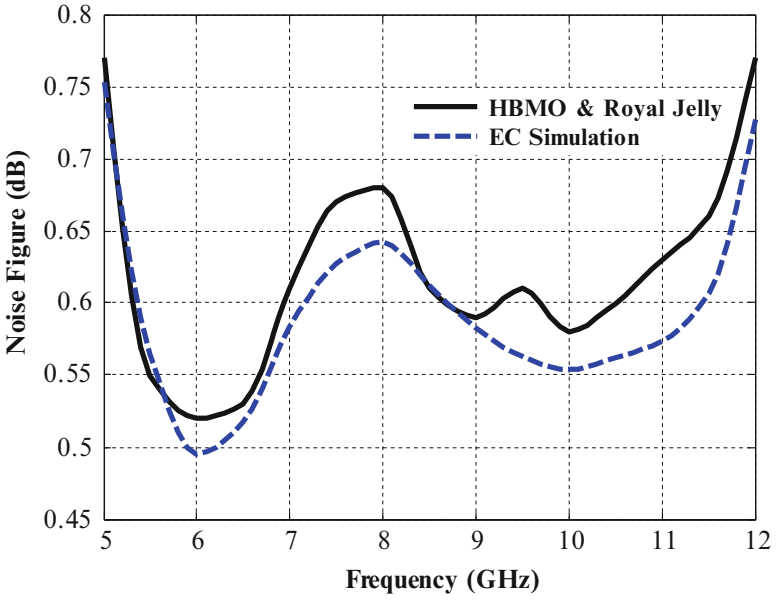

Fig. 12 Synthesized noise performance of the T-type amplifier

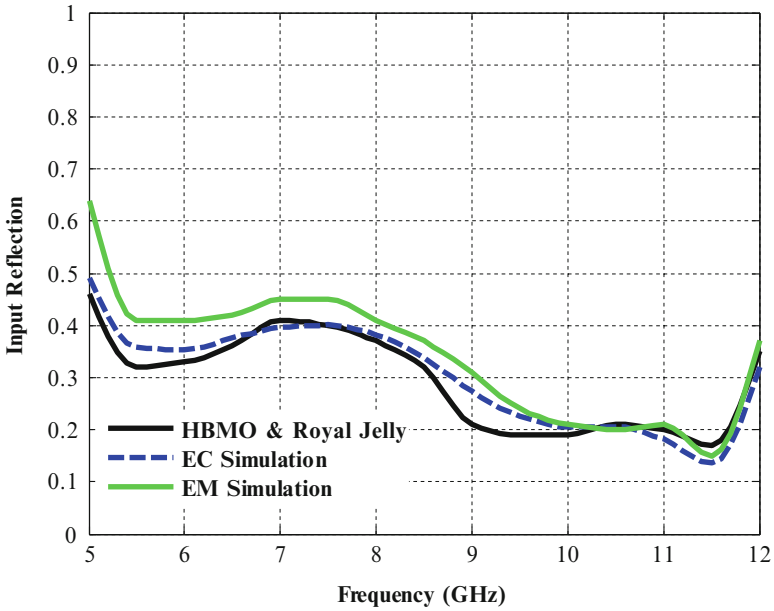

Fig. 13 Input reflection of the T-type amplifier

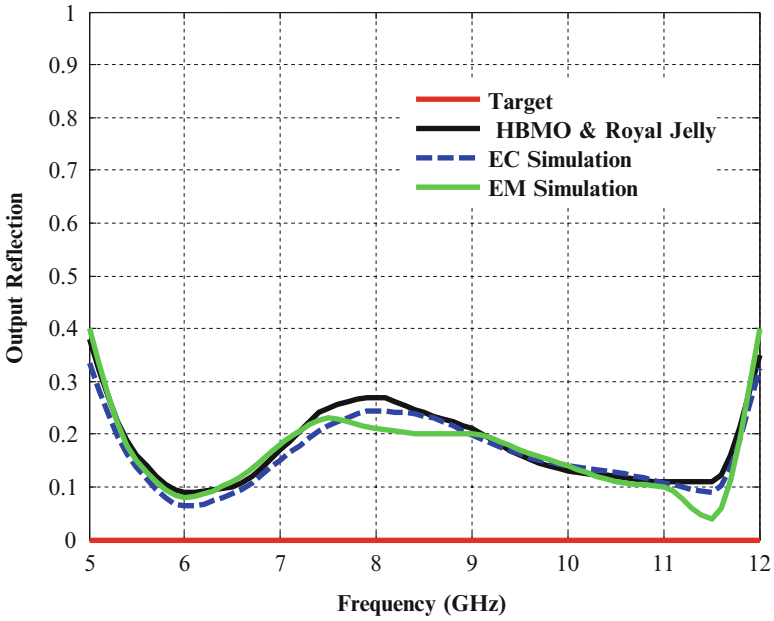

Fig. 14 Output reflection of the T-type amplifier

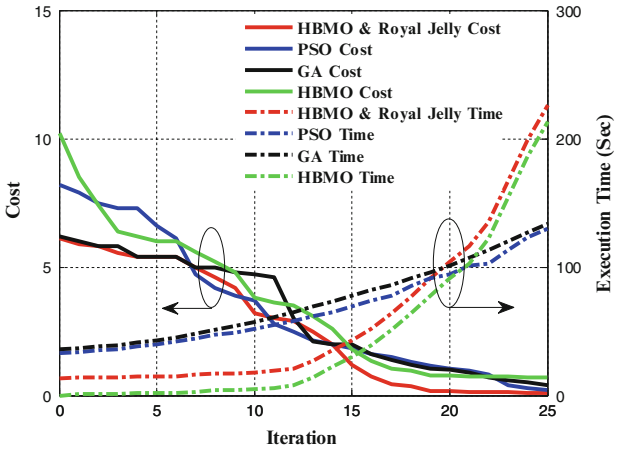

Fig. 15 Cost and execution time variations for PSO, GA, and HBMO and Royal Jelly

Table 3 Benchmarking of cost variation for 10 tries at 20th iteration for all algorithms

Algorithm	Worst	Best	Mean
HBMO and Royal Jelly	0.29	0.12	0.18
HBMO	0.9	0.65	0.74
GA	1.27	0.95	0.99
PSO	1.15	0.9	0.96

Table 4 Solutions of the T-type input and output microstrip matching elements for the maximum output power and the noise figure F(f) = 1 dB

W_1(mm)	W_2(mm)	W_3(mm)	W_4(mm)	W_5(mm)	W_6 (mm)
4.58	4.99	4.32	1.28	3.79	4.13
ℓ_1 (mm)	ℓ_2 (mm)	ℓ_3 (mm)	ℓ_4 (mm)	ℓ_5 (mm)	ℓ_6 (mm)
13.93	5.37	0.77	1.73	5.65	14.36

Table 5 Benchmarking at 20th iteration

Algorithm	Cost	Execution time(Sec)
HBMO and Royal Jelly	0.17	84
HBMO	0.77	71
PSO	1.15	84
GA	1.05	89

Table 6 User-defined parameters of the algorithms

Algorithm	Population	Maximum iteration	Special parameters
HBMO and Royal Jelly	Iteration 5	25	NDrone = 20, Emax = 1, Emin = 0.2, NRJ = ±0.01
HBMO	Iteration 5	25	NDrone = 20, Emax = 1, Emin = 0.2
GA	30	25	Gaussian mutation
PSO	30	25	Learning factors c1 = c2 = 2

1.7 Summary

In this part of the chapter a front-end amplifier is formulated as a constrained optimization problem each ingredient of which is carried out rigorously on the mathematical basis. The significance of the work for the microwave circuit theory can mainly be itemized as follows:

(1) First of all, the design needs solely the fundamental microwave circuit knowledge; (2) Design target is feasible based on the potential performance of the used active device that is obtained by solving numerically the nonlinear gain, noise, and input and output mismatching equation using a metaheuristic algorithm subject to the design objective; (3) In the design of the input and output microstrip matching circuits, the cost effective microstrip SVRM model is used as a fast and accurate model so that it facilitates to obtain directly all the matching microstrip widths, lengths $\left\{\vec{W}, \vec{\ell}\right\}$ on a chosen substrate to satisfy the feasible design target (FDT) over the required bandwidth of a selected transistor; (4) Microstrip matching circuit in any configuration can be easily synthesized by either gradient/nongradient optimization.

It can be concluded that the paper presents an attractive design method for a front-end amplifier design based on the transistor potential performance, and it can be adapted to design of the other types of linear amplifiers.

2 Design Optimization of Reflectarray Antennas

Reflectarray antenna (RA) is able to provide equivalent performance of a traditional parabolic reflector, but their simple structures with the low profiles, light weights, and no need any complicated feeding networks. This can be achieved by designing each RA element to reflect the incident wave independently with a phase compensation proportional to the distance from the phase center of the feed-horn to form a pencil beam in a specified direction (θ_0, ϕ_0) as is well-known from the classical array theory. Thus, "Phasing" is very important process in designing reflectarray. In literature different approaches of compensating the phase of each element have been proposed, however, phasing method using the variable size patches is preferable choice in many designs due to its simplicity [28, 29].

Since it is simple to manufacture the microstrip RA on a single layer, in order to satisfy requirements as the capability to radiate a shaped beam or multi-beams, or also to enhance the frequency behavior and bandwidth, the advanced patch configurations are necessary to be worked out in which the structure has a lot of degrees of freedom and all concur to the performances of the whole antenna. The management of different parameters and the need of satisfying requirements that could be also in opposite each other could however make the design of a reflectarray quite complex. Therefore first of all for a computationally efficient optimization process, an accurate and rapid model for the reflection phase of a unit element is needed to establish it as a continuous function in the input domain of the patch geometry and substrate variables, then it could be convenient to carry this model out adopting a hybrid "global + local" search method to find the best solution among all the possible solutions.

Thus, the systematic design optimization procedure for the Minkowski RA is presented in this chapter. It can briefly be summarized in the following steps: The first step is devoted to the discretization of the 5-D Minkowski space of (m, n, ε_r, h, f) to obtain the training and validation data for MLP NN. In the next part, the gain and bandwidth optimization of MLP NN model with respect to the input variables will be presented using the hybrid combination of Genetic and Nelder-Mead algorithms. In addition, the sensitivity and yield analyses are performed for the tolerance analysis in order to specify the tolerance limits of optimized design parameters. Design and performance analysis of the Minkowski RAs with the optimized or non-optimized antenna parameters will be taken place in the fourth and fifth sections, respectively. Finally the paper ends with the conclusions.

2.1 Reflection Phase Characterization of a Minkowski Element

2.1.1 Minkowski Space

In the design of microstrip RA, the shape and geometry selection of the RA element is the crucial part as well as the substrate properties chosen. In this work, the geometry of radiating element has been proposed to be a resonant element shape for a periodic RA structure, which is a first fractal type, as called the Minkowski shape. Fig. 16a shows the geometrical representation of Minkowski shape patch element.

The relationship between the Minkowski parameters is formulated as:

$$n = \frac{s}{m/3}, \qquad 0 \leq n \leq 1 \tag{9}$$

In Eq. (9), s is the indention and m is the width of the patch, respectively, and n refers the indention ratio. The reflection response of unit cell and phase of reflected wave are generated by the 3-D CST MWS-based analysis implemented

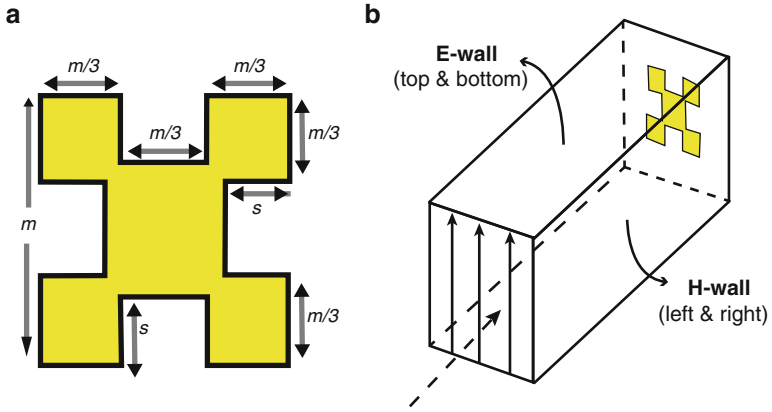

Fig. 16 (**a**) Minkowski patch geometry, (**b**) The H-wall waveguide simulator

to the H-wall waveguide simulator which is shown in Fig. 16b. The top and bottom surfaces of the H-wall waveguide simulator are perfectly electric conducting walls, while the right and left walls are perfectly magnetic field walls [29]. The vertically polarized incoming waves will be incident normally onto the element at the end of the waveguide at the broadside direction and then scattered back also at the broadside direction with a set of amplitude and phase information. The 5-D discretized Minkowski space of (m, n, ε_r, h, f) is constructed by totally 5400 samples to be used in the training and validation of the MLP NN model using the H-wall waveguide simulator analyzed by 3-D CST MWS as follows:

The operation bandwidth of 8–12 GHz is swept as the intervals of 1 GHz and the resulted number of the sample frequencies is fs $=$ 5. Then, Minkowski sampling matrix (Fig. 17) is generated as n s $\times$ ms for each sampled substrate properties (εr, h) at each sampling frequency where n s $=$ 6 and ms $=$ 5 are the number of samples for the indention factor and patch width within the ranges of 0.15 $\leq$ n $\leq$ 0.9 and m $\pm$ (Δm/m) max $=$ m $\pm$ % 20 where m is the resonant length at 11 GHz, respectively. Simultaneously the substrate thickness h is sampled as the intervals of 0.5 mm between them 0.5 mm $\leq$ h $\leq$ 3 mm and the total number of the thickness sampling is h s $=$ 6. In addition, the dielectric permittivity of substrate (εr) is totally sampled εs $=$ 6 times between 1 $\leq$ εr $\leq$ 6. Thus, the entire Minkowski space is discretized totally into the εs $\times$ fs $\times$ hs $\times$ ms $\times$ ns $=$ 5400 Minkowski configurations [30–32].

2.1.2 The Modeling of MLP NN

The employed MLP NN model of Minkowski patch, which is generalization process, is depicted in Fig. 18. The MLP NN has the two hidden layers each of which consists of 10 neurons activating by the tangential sigmoid function. The

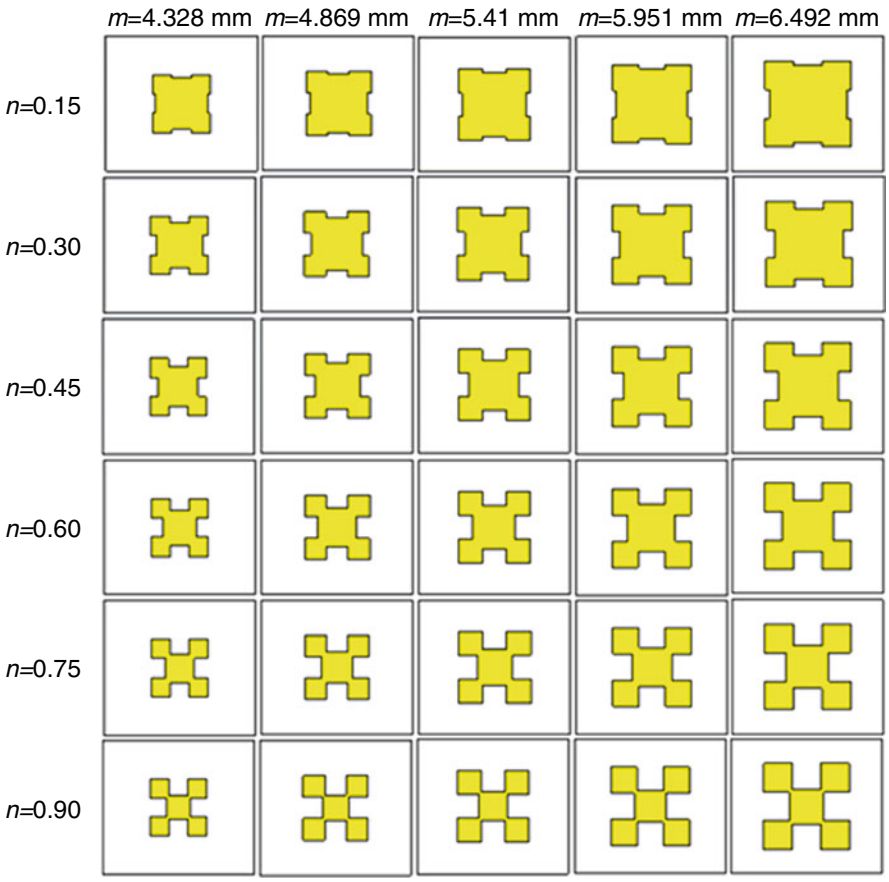

Fig. 17 Sampling Minkowski patch variation matrix (*ns* x *ms* = 6 x 5 = 30)

input and output vectors $\left(\overrightarrow{x}, \overrightarrow{y}\right)$ are 5- and 1-dimensioned, respectively, and can be expressed as Eq. (10):

$$\overrightarrow{x} = [m \;\; n \;\; \varepsilon_r \; h \;\; f]^t, \quad \overrightarrow{y} = [\varphi_{11}]^t = \varphi_{11}\left(\overrightarrow{x}, \overrightarrow{w}\right) \tag{10}$$

where $\overrightarrow{w}$ is the weighting vector of the MLP NN given in Fig. 13. The output function $\varphi_{11}\left(\overrightarrow{x}, \overrightarrow{w}\right)$ can be built using the MLP NN theory [8]. The weighting vector $\overrightarrow{w}$ is determined by the optimization with mean-squared error (Eq. 11) over the training data using the Levenberg-Marquardt algorithm [33, 34]:

$$MSE = \sum_{k \in T_r} \left(\varphi_{11k} - d_k\right)^2 \tag{11}$$

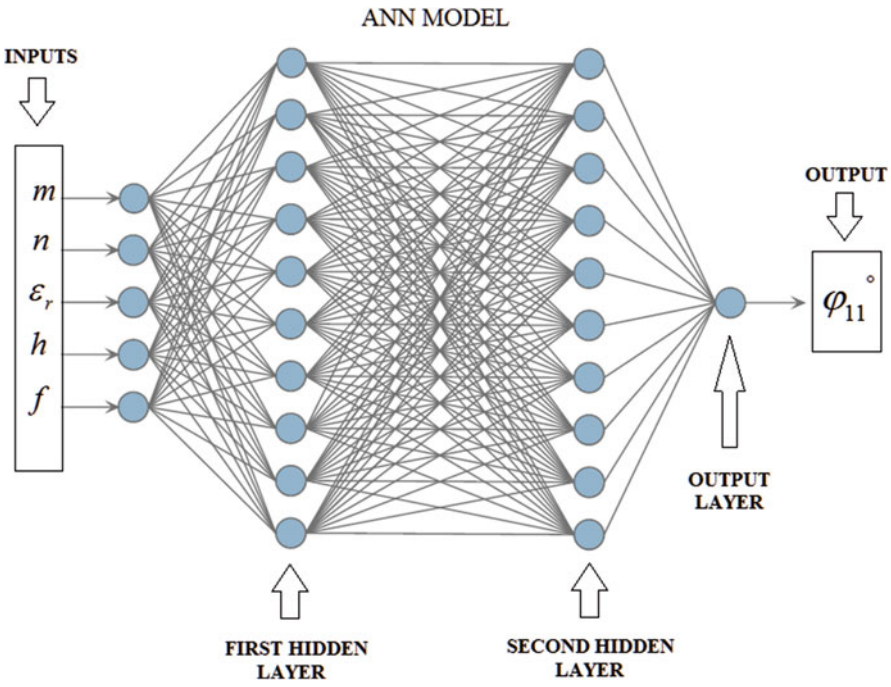

Fig. 18 The MLP NN structure for Minkowski patch

where T_r is an index set of the training data which consists of 3240 $(\vec{x},\ \varphi_{11})$ data pairs corresponding to the patch lengths of 4.328, 5.41, and 6.491, the rest of 2160 $(\vec{x},\ \varphi_{11})$ data pairs are used to validate the MLP NN model. The linear regression scattering plots for the training and the validation process are given with their MSE errors in Fig. 19.

Fig. 20 gives the 3-D view of the reflection phase variations with the patch width m and the relative permittivity of substrate (ε_r) for the constructed and targeted data at the fixed conditions of $h = 1.5$ mm, $n = 0.6$, $f = 11$ GHz. Some examples of modeling performances are depicted in Fig. 21 where the constructed phasing characteristics are compared with their targets. Furthermore thus, it can be inferred that the MLP NN model works very well in generalization of the 5400 $(\vec{x},\ \varphi_{11})$ data pairs to the entire domains to obtain the continuous Minkowski reflection phasing function $\varphi_{11}(\vec{x})$. In the next section, this $\varphi_{11}(\vec{x})$ function will be used directly to determine the phase calibration characteristic and later it will be reversed to synthesize the Minkowski RA in the Memetic optimization procedure.

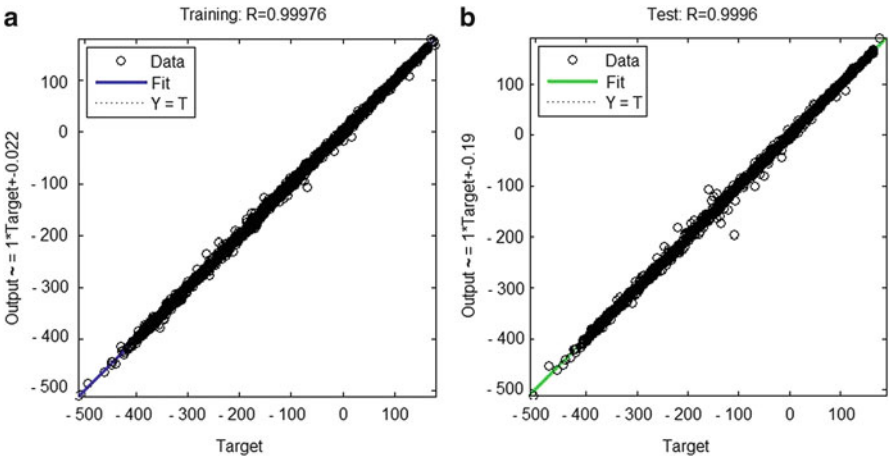

Fig. 19 Regression scattering plots for the complete Minkowski MLP NN model (**a**) training (MSE Error = $9.9564\text{x}10^{-5}$) and (**b**) validation (MSE error = $1.7264\text{x}10^{-4}$)

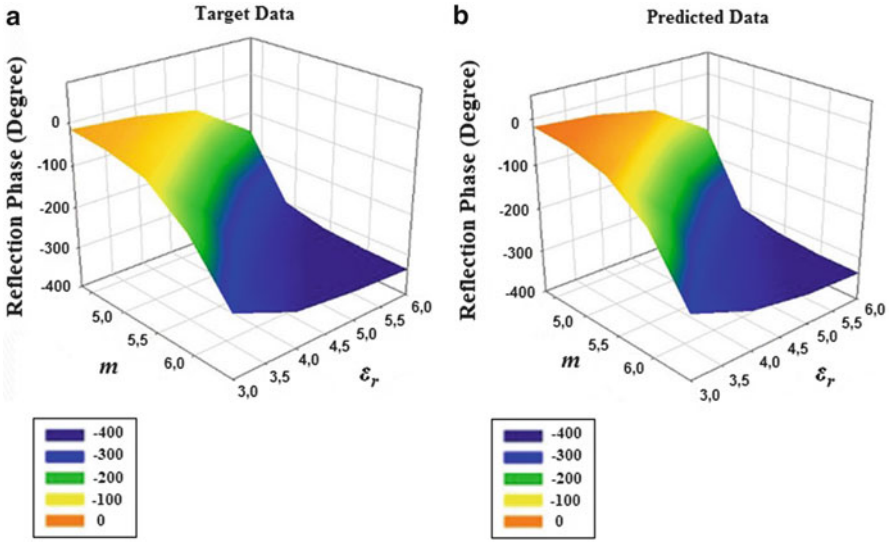

Fig. 20 3-D view of reflection phase variations w.r.t. the patch width m and the relative permittivity ε_r for the fixed conditions of $h = 1.5$ mm, $n = 0.6$, $f = 11$ GHz for (**a**) target and (**b**) constructed data

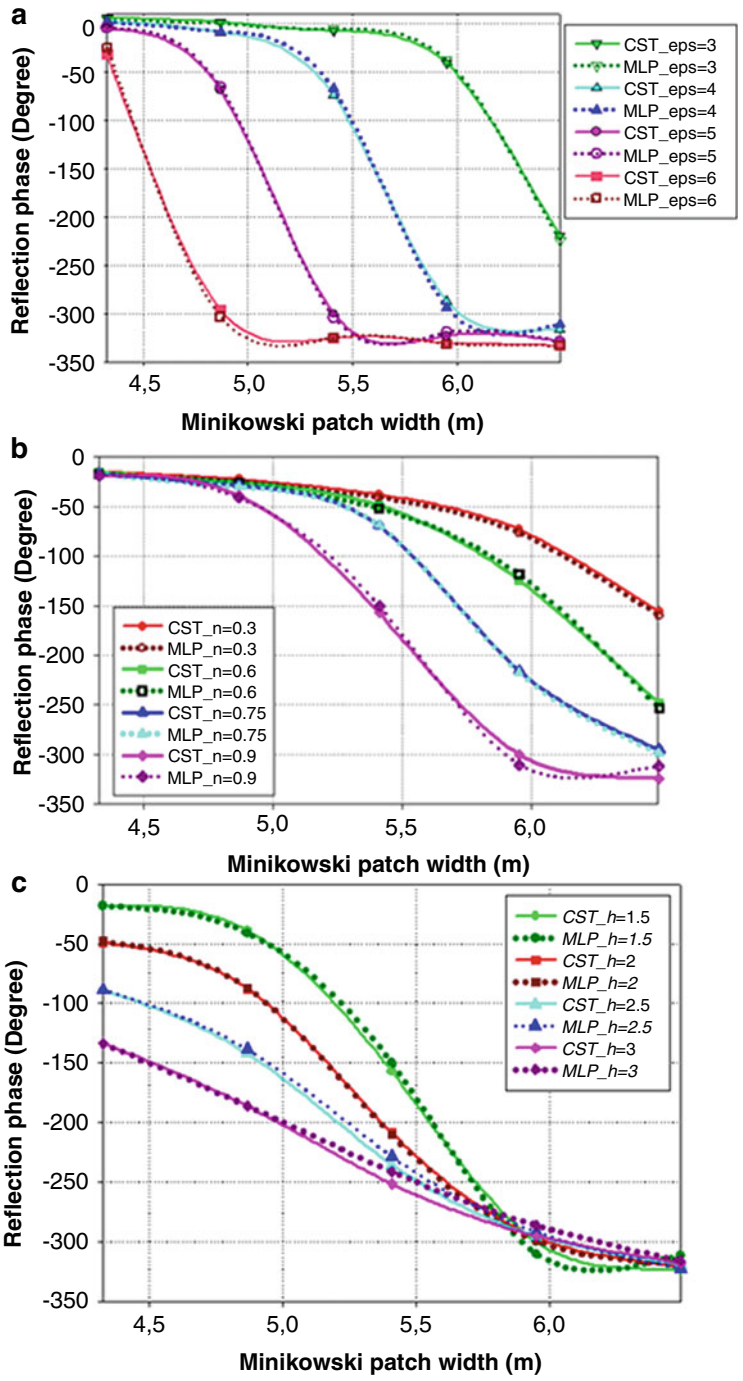

Fig. 21 Reflection phase characteristics for (**a**) $h = 1$ mm, $n = 0.60$, $f = 11$ GHz; taking dielectric constant ε_r as parameter; (**b**) $\varepsilon_r = 3$, $h = 1.5$ mm, $f = 11$ GHz and indention ratio n is parameter (**c**) $\varepsilon_r = 3$, $n = 0.90$, $f = 11$ GHz and substrate thickness h is parameter

2.2 The Optimization Process

2.2.1 Objective Function

In the optimization process, a multi-objective procedure is established where the phase calibration characteristic is selected among the phasing characteristics obtained in the previous section as the one having the slower gradient and the wider range with respect to the indention of patch (n) and substrate (ε_r, h) to achieve the wider band and smaller susceptibility to the manufacturing errors. Thus, this objective can be expressed as the sum of the three ingredients as follows:

$$Objective = \underset{n,\, h,\, \varepsilon_r}{Min} \left\{ \sum_{i=l,c,u} \vartheta_i\,(n,\ h,\ \varepsilon_r) \right\} \tag{12}$$

with the following objective ϑ_i at the frequency f_i:

$$\vartheta_i = \left\{ \sum_{\substack{\varepsilon_r=1 \\ \Delta\varepsilon_r=0.01}}^{6} \ \sum_{\substack{h=0.5\text{mm} \\ \Delta h=0.01\text{mm}}}^{3\ \text{mm}} \ \sum_{\substack{n=0.15 \\ \Delta n=0.01}}^{0.9} W_1.\in_1(f_i) + W_2.\in_2(f_i) + W_3.\in_3(f_i) \right\} \tag{13}$$

where,

$$\in_1 = e^{-\left(\frac{\varphi\max - \varphi\min}{360}\right)} \tag{14}$$

$$\in_2 = |\varphi_{\max} - \varphi_{center}| - |\varphi_{\min} - \varphi_{center}| \tag{15}$$

$$\in_3 = 1\text{-}\left(\frac{\Delta\varphi_{center}}{\Delta m_{center}}\right) \tag{16}$$

In Eq. (14), $\in_1$ is used to maximize the phase range while $\in_2, \in_3$ provide the centralization of the characteristic with the angle of $\pi/4$. In Eqs. (14), (15), and (16), $\varphi_{\max}$, $\varphi_{\min}$, and φ_{center}, are the reflection phase values at m_{max}, $m_{\min}$, and m_{center} for a certain (n, ε_r, h) set, respectively, at the f_i where l, c, u stand for the lower, center, and the upper frequencies. In the optimization process, the operation frequency range is defined as follows: $f_l = 10$ GHz, $f_c = 11$ GHz, $f_u = 12$ GHz. In Eq. (16), the phase difference between $\varphi_{\max}$ and $\varphi_{\min}$ is normalized by dividing 360 and ($\Delta\varphi_{\text{center}}/\Delta m_{\text{center}}$) is the gradient of the phasing characteristic at the point of (φ_{center} ,m_{center}) which is aimed at to be equal to unity corresponding to optimum angle $\pi/4$. All weighting coefficients in the objective function ϑ_i at the frequency f_i

in Eq. (13) have been taken as unity. Optimization process is completed as soon as the iteration number has reached to its maximum value or the predefined cost value. In our case, the optimization ends when the cost value reaches to 0.4353 with the optimized values of all the weighting coefficients.

2.2.2 The Memetic Algorithm: Hybrid Combination of GA-NM Algorithm

A Memetic algorithm (MA) is essentially a combination of a population-based global optimization algorithm with a local search [35]. Recently, Memetic algorithms consisting of the hybrid GA-NM and bacterial swarm optimization BSO-NM algorithms are successfully implemented to designs of the low-noise microwave amplifier and Bow–Tie antennas in [36] and [37], respectively. In this work, a Genetic Algorithm (GA) is used as a population-based global optimizer and a simple local search algorithm called Nelder-Mead (NM) [13] is employed along with the GA to reduce the cost of the solution at each iteration of the optimization procedure.

The GA uses the evolution operations which are the crossover, mutation, and recombination together with the concept of fitness. The population is built by the chromosomes as the solution candidates, binary encoded randomly varied as 0 and 1. The objective function corresponding to each chromosome is evaluated, then chromosomes are ranked according to their fitness's and the least fit ones are discarded and the remaining chromosomes are paired at randomly selected crossover points. In order to prevent the solution from being trapped into the local minima, mutation process is applied by transforming a small percentage of the bits in the chromosome from 0 to 1 or vice versa. The mutation process per iteration is applied for 1 % of the chromosomes.

The MA used in our work can be briefly described through the following abstract description [37]:

Begin
Population initialization
Local search
Evaluation
Repeat
Crossover
Recombination
Mutation
Local Search
Evaluation
Selection
Until termination criterion is satisfied
Return best solution
End

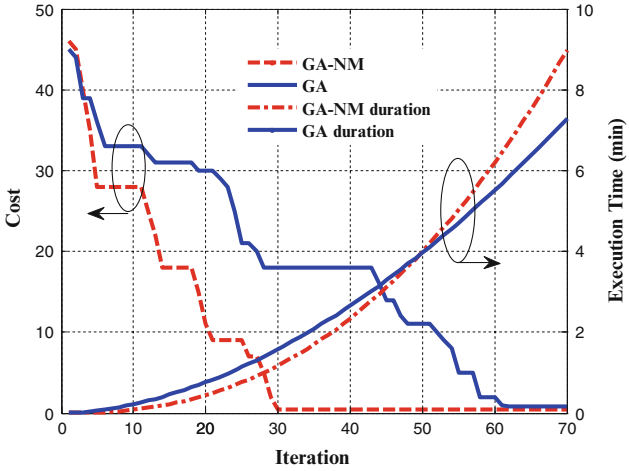

Fig. 22 The convergence curves of the genetic and Memetic optimization

Here, the initial populations are usually generated in a random or controlled manner and then the evolution of these populations is carried out by the genetic operators such as crossover, mutation, and recombination. Local search is utilized to reduce the cost of the resulted solution from the global optimization.

In our GA-NM application, the MATLAB [34] is used for the Memetic algorithm with the selection stochastic uniform operators consisting of a population (chromosome) of 60, number of generation of 900, crossover probability of 0.8 (or crossover fraction for reproduction is 0.8), and mutation probability of 0.001. Mutation function is constraint dependent. Crossover function is scattered. Migration direction is just forward numbered 0.2. The convergence occurs very quickly typically within the 30 iterations shortening 5 times as compared with the 60 iterations GA process, which takes 1 min and 12 s and 5 min and 41 s with Core i7 CPU, 1.60 GHz Processor, 4 GB RAM depending on the initialization values. A typical convergence curve is given in Fig. 22 [38].

2.3 Tolerance Analysis of the Optimized Parameters

The design parameters may usually change in a certain tolerance region during the manufacturing process. Thus it is of interest to which percentage the design specifications are fulfilled. Thus the yield analysis is applied to compute an expected tolerance as percentage. In the implementation of yield analysis, variations in the design parameters are assumed to be small so that the linearization via the sensitivity analysis can be valid. For this reason a yield analysis can only be applied after a successful run of the sensitivity analysis. In the sensitivity analysis, the derivatives

of output function with respect to geometric and/or material design parameters can be calculated without re-meshing the example. The first derivative of the network function with respect to a design parameter can be calculated with the information of the nominal value in a small neighborhood of that nominal value. Also the sensitivity information is used for a more efficient optimization.

In this study, sensitivity analysis is applied to the optimum dielectric constant $\varepsilon_{ropt} = 3.164$ by rounding up the other parameters, as $n_{opt} = 0.85$, $h_{opt} = 1.8$. Then the yield analysis is applied to the results of the sensitivity analysis for the three values of the standard deviation belonging to the dielectric constant. The graphics for these results are shown in Fig. 23 [38].

As is seen from Fig. 23, the best tolerance is at the nominal design parameter value with a lower and upper bound (−3*sigma, +3*sigma) of the dielectric permittivity when the sigma is equal to 0.01. The upper and lower bound indicate as the worst case limits of the tolerance for the dielectric property of substrate. The substrate that has closest specifications to the optimized parameters had been searched, and the two commercially available substrates which are Rogers RO3003 and RO4232 have been found. As is seen from Fig. 24, RO4232 is the fittest substrate as commercially available for our optimized parameter result.

2.4 Design of the Variable–Size RA

2.4.1 Phase Compensation

In this study, the 15×15 variable sizes Minkowski RA with half-wave spacing at resonant frequency of 11 GHz are designed. The radiation analysis has been generated using available full-wave simulation tool of CST MWS. In the phase compensation unit, a coordinate system has been used to determine the progressive phase distribution on the microstrip reflectarray surface of $M \times N$ arbitrarily spaced patches with a centered focal point that will produce a pencil beam in a direction of normal to the surface [8]. Thus, the required phase to compensate path difference $\triangle$R(x) for a reflectarray element can be given as a function of its radial distance x to the center and the operation frequency f as follows:

$$\varphi\,(x,f) = -\beta\,(\Delta R_{\max} - \Delta R(x)) = -\frac{2\pi f}{c} F\left(\sqrt{1+(D/F)^2/4} - \sqrt{1+(x/F)^2}\right) \tag{17}$$

where the minus sign expresses delay, c is the velocity of light. In Eq. (17) D and F are the diameter and the focal length of the feed to the array center, respectively. Quadrature symmetry characteristic of the phase compensation with respect to the element position for the 15×15 reflectarray where frequency is considered as the parameter and F/D is taken as 0.8.

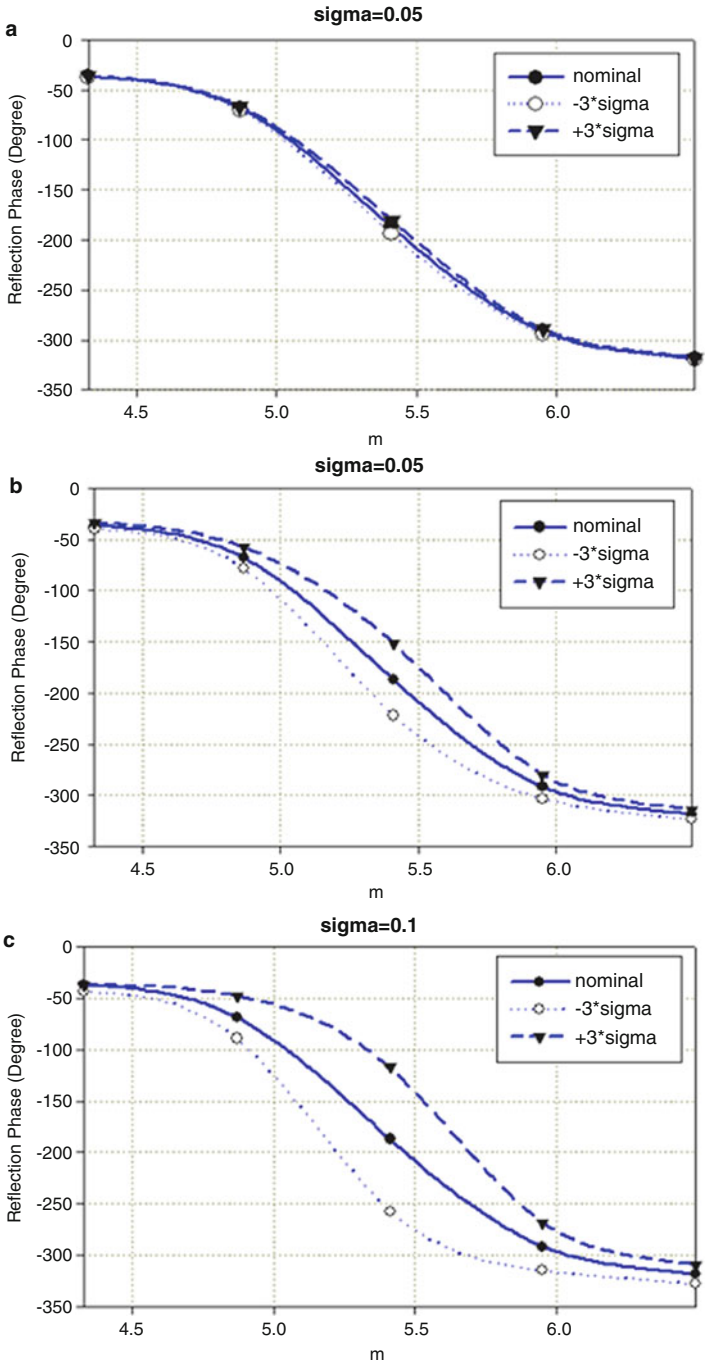

Fig. 23 Sensitivity analysis results for the optimum dielectric constant for the standard deviation (sigma) values: (**a**) $\sigma = 0.01$, (**b**) $\sigma = 0.05$, (**c**) $\sigma = 0.1$ at $f = 11$ GHz

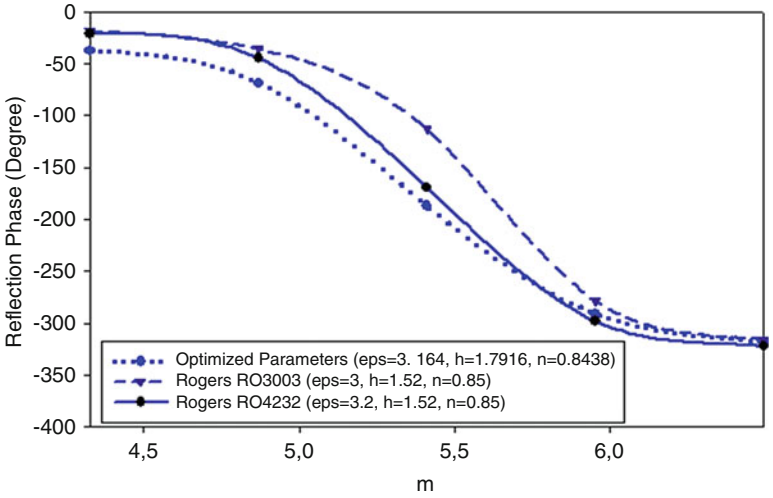

Fig. 24 Comparison of the reflection phase responses for unit cell element designed with optimized parameters and two equivalent commercially available substrates

2.4.2 Determination Size of Each Radiator

Size of each radiator is determined to meet the necessary compensation phase using the phase calibration characteristic. For this purpose, the established ANN model is reversed by inputting optimum values corresponding to the phase calibration characteristic and while input m changes itself using the adaptable size $\triangle m$ which get exponentially smaller with an adaptation parameter τ as decreasing the squared error as given in Fig. 25 [32].

2.5 Implementation

In the implementation stage, all the radiation performance analyses are made using 3-D CST Microwave Studio. The fully optimized X-band Minkowski reflectarray antenna with the parameters $\varepsilon_{\text{ropt}} = 3.1694$, $h_{opt} = 1.7916$ mm, $n_{opt} = 0.8438$ is designed using the general design procedure (Fig. 25) and its realized gain patterns at the frequencies 10.5, 11, and 11.9 GHz are given in Fig. 26a. Furthermore for the purpose of comparison, the realized gain patterns of an arbitrary non-optimized RA antenna with the parameters of $\varepsilon_r = 2.2$, $h = 1.5$ mm, $n = 0.90$ at the same frequencies are obtained with the same procedure and depicted in Fig. 26b and the compared performance values take place in Tab. 7. In order to examine the influence of dielectric property optimization, the gain variation with respect to the frequency is obtained with the same optimized indention ratio $n_{opt} = 0.8438$ and thickness $h_{opt} = 1.7916$ mm, but on some traditional substrates which are Taconic RF-35 with

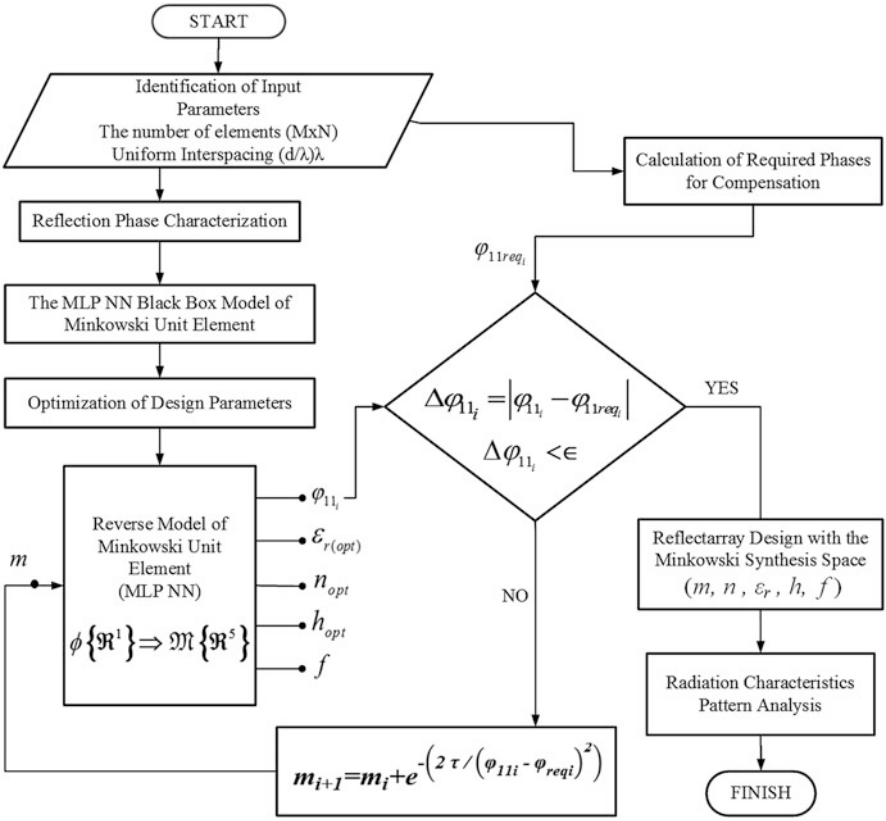

Fig. 25 Design flow chart for the optimum reflectarray antenna

$\varepsilon_r = 3.5$, Taconic TRF41 with $\varepsilon_r = 4.1$, Rogers TMM4 with $\varepsilon_r = 4.5$ and depicted in Fig. 27. The performance values corresponding to Fig. 27 take place in Tab. 8, Fig. 28 depicts the gain versus frequency variations of the optimized RAs designed on the dielectric $\varepsilon_{ropt} = 3.1694$ and the traditional substrates. The performance values belonging to Fig. 28 are given in Tab. 8 (Tab. 9).

2.5.1 Summary

Doubtlessly, microstrip reflectarrays are of prime importance in today's antenna technology, since they combine the advantages of both the printed phased arrays and parabolic reflectors to create a new generation of high gain antennas.

In this part of the chapter, a robust and systematic method is put forward to be used in the design and analysis of a Minkowski reflectarray. The most important and critical stage of a reflectarray design is the design optimization of its element.

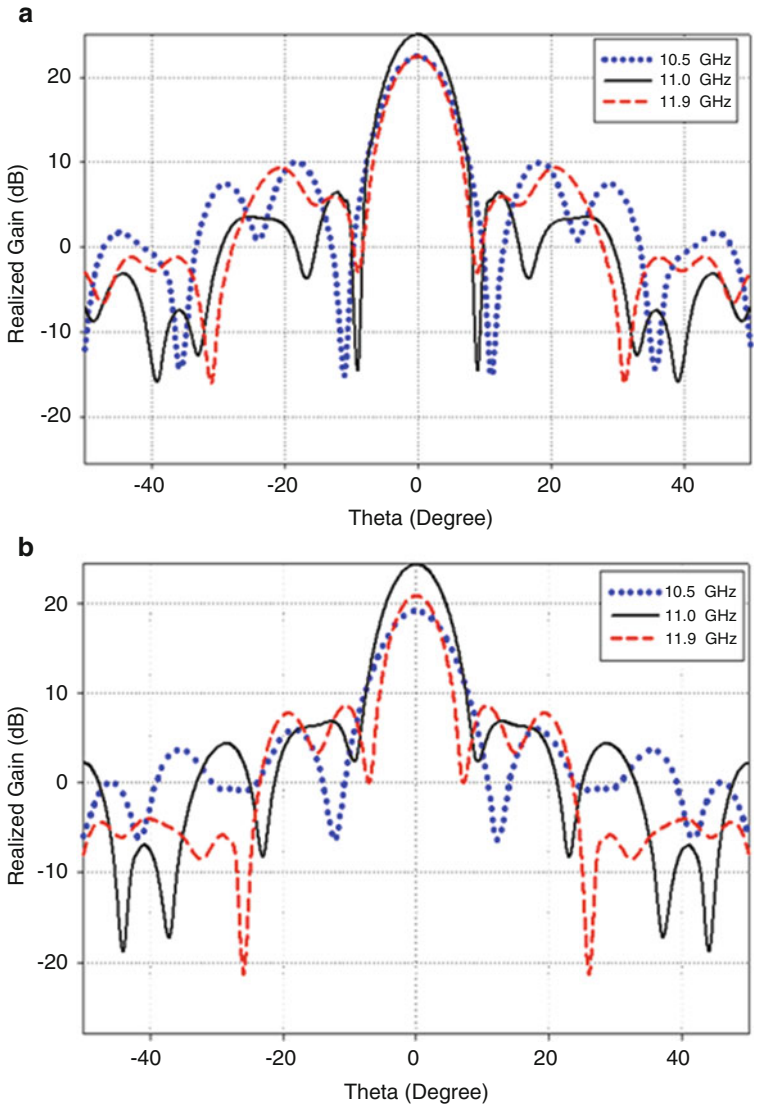

Fig. 26 (**a**) Fully optimized RA with $\varepsilon_{ropt} = 3.1694$, hopt = 1.7916 mm, nopt = 0.8438; (**b**) Non-optimized reflectarray with $\varepsilon_r = 2.2$, h = 1.5 mm, n = 0.90

Therefore, firstly a complete, accurate and fast MLP ANN model of a Minkowski patch radiator is built based on the 3-D CST Microwave Studio MWS that takes into account all the main factors influencing the performance of the Minkowski RA. When the outputs of performed MLP ANN model and 3-D simulations are compared, it is verified that the MLP is very accurate and fast solution method to construct the highly nonlinear phasing characteristics within the continuous domain

Table 7 Performance comparison of the fully optimized reflectarray with a non-optimized reflectarray

Antenna	Frequency (GHz)	Realized gain (dB)	Side lobe level (dB)	Angular width (3 dB) (Deg.)
Optimized RA $\varepsilon_{ropt} = 3.1694$, $h_{opt} = 1.7916$, $n_{opt} = 0.8438$	10.5	22.5	−12.5	7.9
	11	25	−18.6	7.4
	11.9	22.5	−13.2	7.1
Non-optimized RA $\varepsilon_r = 2.2$, $h = 1.5$, $n = 0.90$	10.5	19.2	−13.2	8.8
	11	24.4	−17.5	7.5
	11.9	21	−12.4	6.3

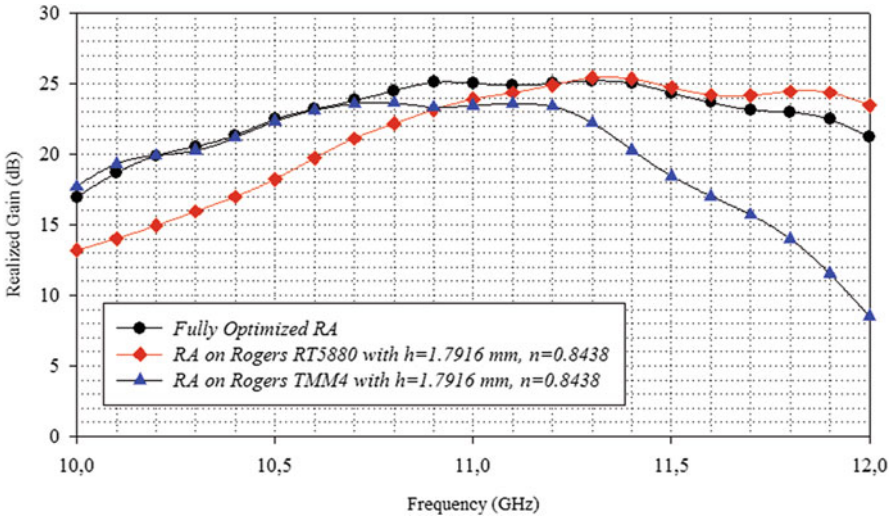

Fig. 27 Realized gain versus frequency graphs for the fully optimized RA and the other RAs on the different substrates with the optimized parameters n_{opt}, h_{opt}

of the geometrical and substrate parameters of the RA element and frequency. All the stages of building the MLP ANN model and its utilization in design of a Minkowski RA are given in details as a general systematic method that can be applied to the differently shaped patch radiators.

Overall parameters of Minkowski RA including dielectric permittivity of the substrate ε_r are optimized for an optimum linear phasing range of an ultra-wideband RA in the X-band by applying a standard novel evolutionary hybrid combination of Global Genetic (GA) and Local Nelder-Mead (NM) algorithms.

In addition to optimization process, the sensitivity and yield analyses are performed as tolerance analysis in order to specify the tolerance limits of optimized design parameters and the commercially available substrate options which are compatible with our optimized design parameters. The optimum dielectric permittivity

Table 8 Comparison of the fully optimized RA and the other RAs designed on the different substrates with same optimized parameters n_{opt}, h_{opt}

	Realized gain (dB)		
Frequency (GHz)	Fully optimized RA $\varepsilon_{ropt} = 3.1694$, $h_{opt} = 1.7916$ mm, $n_{opt} = 0.8438$	Rogers RT5880 $\varepsilon_r = 2.2$, $h_{opt} = 1.7916$ mm, $n_{opt} = 0.8438$	Rogers TMM4 $\varepsilon_r = 4.5$, $h_{opt} = 1.7916$ mm, $n_{opt} = 0.8438$
10	17	13.2	17.7
10.5	22.5	18.2	22.3
11	25	23.9	23.5
11.5	24.3	24.7	18.5
12	21.2	23.5	8.5

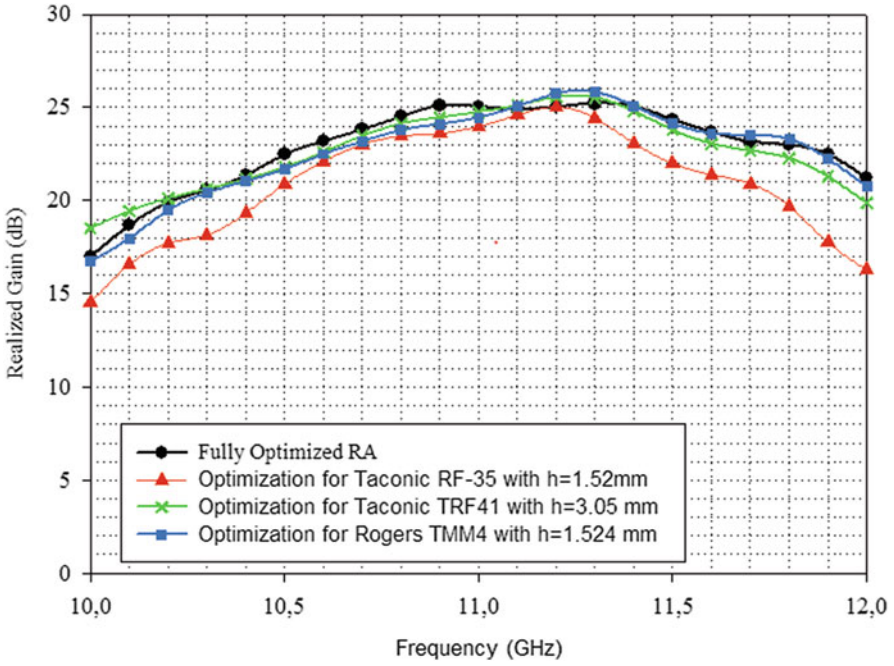

Fig. 28 Gain variations of fully optimized RA with only patch geometry n_{opt} optimized RAs on the given dielectric permittivity ε_r and substrate thickness η

tolerance limits are qualified rounding up the values of the optimum substrate thickness h_{opt} and indention ratio of Minkowski microstrip patch n_{opt} for the three characteristic values of the standard deviation. Thus this tolerance analysis results in the limits of design parameters and the proper commercial available dielectric substrate as Rogers RO4232. Finally, a fully optimized 15×15 Minkowski RA is designed as a worked example. Thus, its radiation characteristics are analyzed

Table 9 Comparison of the fully optimized RA and RAs with the optimized Minkowski shapes on the traditional substrates

Frequency (GHz)	Realized gain (dB)			
	Optimized reflectarray $\varepsilon_{ropt} = 3.1694$, $h_{opt} = 1.7916$, $n_{opt} = 0.8438$	Taconic RF-35 $\varepsilon_r = 3.5$, $h = 1.52$, $n_{opt} = 0.7848$	Taconic TRF41 $\varepsilon_r = 4.1$, $h = 3.05$, $n_{opt} = 0.6212$	Rogers TMM4 $\varepsilon_r = 4.5$, $h = 1.524$, $n_{opt} = 0.3604$
	17	14.5	18.5	16.7
10.5	22.5	20.9	21.8	21.7
11	25	24	24.8	24.5
11.5	24.3	22	23.8	24.1
12	21.2	16.3	19.9	20.7

based on the 3-D CST Microwave Studio MWS and graphically represented, then compared with the performances of the non-optimized and the partially optimized Minkowski RAs.

It may be concluded that the presented method can be considered as a robust and systematic method for the design and analysis of a microstrip reflectarray antenna built by the advanced patches.

References

1. Güneş, F., Gürgen, F., Torpi, H.: Signal - noise neural network model for active microwave device. IEE Proc. Circuits Devices Syst. **143**, 1–8 (1996)
2. Güneş, F., Torpi, H., Gürgen, F.: A multidimensional signal-noise neural network model for microwave transistors. IEE Proc. Circuits Devices Syst. **145**, 111–117 (1998)
3. Giannini, F., Leuzzi, G., Orengo, G., Albertini, M.: Small-signal and large-signal modelling of active Devices using CAD-optimized neural networks. Int. J. RF Microw. Comput. Aided Eng. **12**, 71–78 (2002)
4. Güneş, F., Türker, N., Gürgen, F.: Signal-noise support vector model of a microwave transistor. Int. J. RF Microw. Comput. Aided Eng. **17**, 404–415 (2007)
5. Marinkovic, Z.Z., Pronic -Rancic, O., Markovic, V.: Small-signal and noise modelling of class of HEMTs using knowledge-based artificial neural networks. Int. J. RF Microw. Comput. Aided Eng. **23**, 34–39 (2013)
6. Güneş, F., Özkaya, U., Uluslu, A.: Generalized neural-network based efficient noise modelling of microwave transistors. In: International Symposium on Innovations in Intelligent Systems and Applications (INISTA), pp. 212–216, Istanbul, Turkey, 15–18 June 2011
7. Mahouti, P., Güneş, F., Demirel, S., Uluslu, A., Belen, M.A.: Efficient scattering parameter modeling of a microwave transistor using generalized regression neural network. in Microwaves, Radar, and Wireless Communication (MIKON), 2014, 20th International Conference on, pp. 1–4, 16–18 June 2014
8. Güneş, F., Güneş, M., Fidan, M.: Performance characterisation of a microwave transistor. IEE Proc. Circuits Devices Syst. **141**(5), 337–344 (1994)
9. Güneş, F., Çetiner, B.A.: A Novel Smith chart formulation of performance characterisation for a microwave transistor. IEE Proc. Circuits Devices Syst. **145**(6), 419–428 (1998)

10. Güneş, F., Bilgin, C.: A generalized design procedure for a microwave amplifier: a typical application. Prog. Electromagn. Res. B, **10**, 1–19 (2008)
11. Edwards, M.L., Cheng, S., Sinsky, J.H.: A deterministic approach for designing conditionally stable amplifiers. IEEE Trans. Microw. Theory Tech. **43**(1), 1567–1575 (1995)
12. Demirel, S.: A generalized procedure for design of microwave amplifiers and its applications. PhD Thesis (in Turkish), Yıldız Technical University, Istanbul, Turkey (2009)
13. Demirel, S., Güneş, F.: Performance characterisation of a microwave transistor for maximum output power and the required noise. IET Circuits Devices Syst. **7**(1), 9–20 (2013)
14. Ciccognani, W., Longhi Patrick, E., Colangeli, S., Limiti, E.: Constant mismatch circles and application to low-noise microwave amplifier design. IEEE Trans. Microw. Theory Tech. **61**(12), 4154–4167 (2013)
15. Güneş, F¸Özkaya, U., Demirel, S.: Particle swarm intelligence applied to determination of the feasible design target for a low-noise amplifier. Microw. Opt. Technol. Lett. **51**(5), 1214–1218 (2009)
16. Mahouti, P., Güneş, F., Demirel, S.: Honey– bees mating algorithm applied to feasible design target space for a wide– band front–end amplifier. In: ICUWB 2012- IEEE International Conference on Ultra-Wideband, pp. 251–255 (2012). doi: 10.1109/ICUWB.2012.6340406
17. Güneş, F., Demirel, S., Mahouti, P.: Design of a Front–End Amplifier for the Maximum Power Delivery and Required Noise by HBMO with Support Vector Microstrip Model. Radioengineering, **23**(1), (2014)
18. Tokan, N.T., Güneş, F.: Knowledge –based support vector synthesis of the microstrip lines. Prog. Electromagn. Res. **92**, 65–77 (2009)
19. Güneş, F., Tokan, N.T., Gürgen, F.: A knowledge-based support vector synthesis of the transmission lines for use in microwave integrated circuits. Expert Syst. **37**, 3302–3309 (2010)
20. Güneş, F., Cengiz, Y.: Optimization of a microwave amplifier using neural performance data sheets with genetic algorithms. In: International Conference on Artificial Neural Networks (ICANN), Istanbul, pp. 26–29, June 2003
21. Cengiz,Y., Göksu, H., Güneş, F.: Design of a broadband microwave amplifier using neural performance data sheets and very fast simulated reannealing. In: Wang, J. et al. (ed.) Advances in neural networks – ISNN, Pt3, Proceedings, vol. 3973, pp. 815–820. Springer-Verlag, Berlin, Heidelberg (2006)
22. Güneş, F., Demirel, S.: Gain gradients applied to optimization of distributed-parameter matching circuits for a microwave transistor subject to its potential performance. Int. J. RF Microw. CAE **18**, 99–111 (2008)
23. Güneş, F., Demirel, S., Özkaya, U.: A low-noise amplifier design using the performance limitations of a microwave transistor for the ultra-wideband applications. Int. J. RF Microw. Comput. Aided Eng. **20**, 535–545 (2010)
24. Cengiz, Y., Kılıç, U.: Memetic optimization algorithm applied to design microwave amplifier for the specific gain value constrained by the minimum noise over the available bandwidth. Int. J RF Microw. Comput. Aided Eng. **20**, 546–556 (2010)
25. Keskin, A.K.: Design optimization of ultrawide band microstrip amplifier using 3D Sonnet-based SVRM with particle swarm intelligence. MSc thesis, Yıldız Technical University, Istanbul, Turkey (2012)
26. Güneş, F., Demirel, S., Mahouti, P.: Design of a front– end amplifier for the maximum power delivery and required noise by HBMO with support vector microstrip model. Radioengineering **23**(1), 134–142 (2014)
27. Pozar, D.M.: Microwave Engineering. Wiley, New York (2012)
28. Pozar, D.M., Metzler, T.A.: Analysis of a reflectarray antenna using microstrip patches of variable size. Electron. Lett. **27**, 657–658 (1993)
29. Huang, J., Encinar, J.A.: Reflectarray Antennas. Wiley-IEEE Press, Hoboken. New Jersey. ISBN: 978–0470–08491–4, 2007

30. Nesil, S., Güneş, F., Özkaya, U.: Phase characterization of a reflectarray unit cell with Minkowski shape radiating element using multilayer perceptron neural network. In: 7th International Conference on Electrical and Electronics Engineering (ELECO), pp. 219–222, 1–4 December 2011
31. Nesil, S., Güneş, F., Kaya, G.: Analysis and design of X-band Reflectarray antenna using 3-D EM-based artificial neural network model. In: ICUWB, IEEE International Conference on Ultra-Wideband, pp. 532–536, 17–20 September 2012
32. Güneş, F., Nesil, S., Demirel, S.: Design and analysis of Minkowski reflectarray antenna using 3-D CST microwave studio-based neural network model with particle swarm optimization. Int. J. RF Microw. Comput. Aided Eng. **23**, 272–284 (2013)
33. Zhang, Q.J., Gupta, K.C.: Models for RF and Microwave Components. Neural Networks for RF and Microwave Design. Artech House, Norwood, MA (2000)
34. MATLAB and Neural Networks Toolbox Release: The Math Works, Inc., Natick, Massachusetts, United States (2012b)
35. Konstantinidis, A., Yang, K., Chen, H.-H., Zhang, Q.: Energy-aware topology control for wireless sensor networks using Memetic algorithms. Elsevier Comput. Commun. **30**, 2753–2764 (2007)
36. Mahmoud, K.R.: Design optimization of a bow-tie antenna for 2.45GHz RFID readers using a hybrid BSO- NM algorithm. Prog. Electromagn. Res. **17**, 100–105 (2010)
37. Nelder, J.A., Mead, R.: A simplex method for function minimization. Comput. J. **7**, 308–313 (1965)
38. Güneş, F., Demirel, S., Nesil, S.: Novel design approach to X-Band Minkowski reflectarray antennas using the full-wave EM simulation-based complete neural model with a hybrid GA-NM Algorithm. Radioengineering **23**(1), 144–153 (2014)